Multi-criteria investigation of a Pumped Thermal Electricity Storage (PTES) system with thermal integration and sensible heat storage

Authors
Guido Francesco Frate*, Lorenzo Ferrari, Umberto Desideri
Department of Energy, Systems, Territory and Construction Engineering (DESTEC), University of Pisa, Largo Lucio Lazzarino, Pisa 56122, Italy

Abstract
In the present paper a multicriteria analysis of a Rankine Pumped Thermal Electricity Storage (PTES) system with low-grade thermal energy integration is performed. The system is composed by an ORC for the discharging phase and a high-temperature heat pump for the charging phase. As previously demonstrated, the low-grade thermal energy can be provided at the heat pump evaporator to boost the PTES performances. As regards the multi-criteria analysis, a tradeoff is required when electric-to-electric efficiency η_{rt}, total exergy exploitation efficiency ψ_{ut} and energy density ρ_{en}, are maximized concurrently. By means of multi-objective optimization, theoretical performances of the system are derived in two different layouts, which differ for the presence or not of internal regeneration in charge and discharge subsystems. Results showed that regeneration can be very effective, as it relaxes the tradeoff between the objectives, thus yielding better global performances. Pareto fronts are built and explored to characterize the PTES system. Configurations of interest are proposed, and PTES performances are compared with other storage technologies. Theoretical results showed that, by exploiting thermal energy at temperature lower than 80 °C, $\eta_{rt} \approx 0.57$ and $\rho_{en} \approx 17$ kWh/m^3 can be concurrently achieved. This can be done at the cost of an inefficient exploitation of the thermal source, as $\psi_{ut} \approx 0.07$. If higher total exergy utilization efficiency is required, storage density can be still maintained high, but η_{rt} must drop down to 0.4.

Nomenclature

Symbols:

COP	coefficient of performance, [-]
cp	constant pressure specific heat capacity, [kJ/kg K]
h	enthalpy, [kJ/kg]
LB	lower bound vector
$\dot{m}$	mass flow rate, [kg/s]
p	pressure, [bar]
PP	heat exchanger pinch point, [°C]
$\dot{Q}$	heat flux, [kJ/s]
s	entropy, [kJ/kg K]
T	temperature, [°C]
UB	upper bound vector
W	objective weight
x	optimization variable vector

Subscripts and Superscripts:

0	reference state (20 °C, 1 bar)
air	air
cd	condenser
cmp	compressor
el	electro-mechanical
en	energy
ev	evaporator
exp	expander
fan	cooling fan
gen	generator
hp	heat pump
in	inlet
liq	liquid
max	maximum
min	minimum
mot	motor
non-reg	non-regenerated layout
orc	organic Rankine cycle
out	outlet
pmp	pump
ref	reference point
reg	regenerated layout
rg	regenerator
rt	round-trip
sat	saturated liquid or vapor
sc	subcooling
sf	scalarizing function
sh	superheating
src	heat source
stg	thermal storage
ut	heat source utilization
vap	vapor

Greek symbols:

α	augmentation factor
$\Delta(\cdot)$	difference of $(\cdot)$
η	efficiency

ρ	density, [kJ/m^3] or [kg/m^3]	ψ	exergy efficiency
τ	heat source or heat pump operating time		
χ	steam quality		

1. Introduction

Pumped thermal electricity storage (PTES) is a broad definition which includes a group of technologies which are used to store electric energy as thermal energy. The charge phase is made with different heat pump technologies converting electric energy from renewable energy sources to thermal energy is stored as sensible or latent heat. The discharge phase is performed using different thermal engine technologies [1]. Most of the time, both hot and cold reservoirs are used, but sometimes one of the two is replaced by the environment, or by alternative heat sources [2,3].

Since the PTES mostly relies on well-known technologies (pumps, compressors, expanders, turbines and heat exchangers) that traditionally scale-up well, both in terms of size and cost, the PTES has been proposed as an alternative to Pumped Hydro Energy Storage (PHES, whose name PTES voluntarily mimics) and to Compressed Air Energy Storage (CAES). Compared to these two, PTES typically shows lower roundtrip efficiencies, but, since it does not rely on peculiar geographical configurations, like water reservoirs and geological cavities, it might have some strategical advantages over these technologies.

Broadly speaking, PTES technologies can be divided into two main families and both come in with many slightly different configurations. The first family is based on Brayton cycles (direct and inverse), while the second is based on Rankine cycles (direct and inverse). As for Brayton PTES, the use of both dynamic (see [4], for example) and volumetric machineries [5] have been proposed. This storage technology is most often based on sensible heat storage, which is generally made up of solid materials like concrete, Al_2O_3 or others [6]. Brayton PTES has been extensively analyzed from the thermal, dynamic and economic point of views [7–9]. For storage materials, turbomachinery and working fluids, Brayton PTES has some similarities with the adiabatic CAES (ACAES), which stores compression excess heat similarly to PTES [10]. However, PTES relies more on storing the heat, rather than mechanical energy, so the hot reservoir is generally operated at much lower pressure than in CAES [1].

Although less common than the Brayton counterpart, Rankine PTES has been recently proposed and could be a valid alternative. Rankine PTES generally features higher energy density, due to the use of latent heat storage. The efficiencies practically achievable by the two versions are similar: for Rankine-based versions a round-trip efficiency of 62% is claimed in [11,12], and of 65% in [13]. These figures are similar to those reported in [4] for the Brayton PTES.

The most common Rankine PTES configuration relies on trans-critical and super-critical CO_2 Heat Pumps (HPs) and CO_2 Rankine cycles [11,12]. Additional modifications can be found in [13], where liquid piston nearly-isothermal compression and expansion are introduced.

The concept of using Rankine cycles is not limited to CO_2 configuration. For example, in [14] a cascaded NH_3/Water vapor compression High Temperature HP (HTHP) is used for charging a hybrid sensible/latent heat storage, while the discharge phase is entrusted to a water steam cycle. Although the system proposed by [14] might result too complex to be feasible in practice[1], it introduces the concept of integrating vapor compression HTHPs in PTES systems, which is very interesting. This opens the way for the exploitation of additional heat sources, leading to solutions which might be based on solutions like multi-temperature HPs [15], if the cold reservoir is to be maintained. Otherwise, the cold reservoir could be eliminated thanks to the integration of conventional vapor compression HTHPs, as proposed in [2,3]. Focusing on the application of vapor compression heat pumps in PTES systems, the idea is to decouple the temperature levels of the HP and of the heat engine, by using a low-grade heat source ($T_{source} \leq 80$ °C) to feed the HP evaporator. The energy provided by the heat source is then upgraded by the HP and stored in the hot reservoir. Heat upgrading is an emerging technique in the field of the industrial waste heat recovery, and some HTHPs especially designed for this purpose are already being commercialized [16,17]. In the discharge phase, the storage provides the stored heat to the engine, which later rejects it to the environment. The absence of the cold reservoir stems from the fact that the HP works between the low-grade heat source and the hot reservoir, so the cold reservoir cannot be "charged", and its role is then performed by the environment itself.

Since maximum HTHP temperature level achievable in practice may reach 180 °C, this was assumed as the maximum temperature level of the storage in this configuration. Therefore, the engine technology must be

[1] Compression is performed with nine liquid-injected compression stages. Round trip efficiency resulted to be around 73%, but it its calculated with compressor polytropic efficiency equal to 0.9, which might not be realisable in practice.

selected among those suited for low-temperature waste-heat recovery. The most mature, widespread and performing of such technologies is represented by Organic Rankine Cycles (ORCs).
Both HTHPs and ORCs are widely studied systems and these last years of research demonstrated how a proper choice of working fluid and cycle architecture may deeply affect their performance [18]. As far as PTES systems are concerned, charge and discharge devices must be optimized together, as the operational conditions which maximize HP COP are not those which maximize ORC efficiency, and vice versa. Since roundtrip efficiency depends on both, a trade-off must be achieved. similarly, the choice of working fluid pair cannot a priori rely on the fluids that are normally used for HTHPs and ORCs applications. In fact, the resulting cycle arrangements could mismatch when coupled together through the thermal storage. Nonetheless, fluid choice can be somewhat guided by previous researches and the pool of potential working fluids can be substantially restricted based on previous analysis, such as [18], where a detailed screening of HTHP working fluid performance is carried out. Likewise, if the basic architecture is to be modified, the choice can be realistically restricted to those architectures that already proved to bring advantages which overcome the additional expenditures. For both HTHPs and ORCs, such architectures, are those which feature internal regeneration [16,19]. Since these architectures are emerging as a new standard in HTHP and ORC applications, it can be concluded that they can be justified in terms of capital expenditure and performance increments. Therefore, a "regenerated" PTES is compared with the basic one in the analysis.
The concept of Thermal Integration (TI), i.e. the use of low-grade heat sources to boost the performances of PTES systems, is briefly cited in [14,20], but the first in-depth analysis, has been performed in [3], to the best of the authors' knowledge. Additional details can be found also in [2]. Such papers ([2,3]) deal with a particular TI-PTES concept, which is essentially the integration of additional low grade heat sources to eliminate PTES cold reservoir. Nonetheless, the opposite can be done, as reported in [21], where the use of the heat source to substitute the hot reservoir, while maintaining the cold one, has been investigated.
In [2,3] a PTES system with vapor compression HTHP, regenerated ORC and ideal latent heat hot reservoir, was analyzed. Several combinations of HP and ORC working fluids were tested and maximum round-trip efficiency η_{rt} (defined as the ratio between the electric energy absorbed by the HP and that returned by the ORC) was calculated in function of the heat source and hot reservoir temperature levels.
Although η_{rt} is of a paramount importance for storage systems, previous analyses are somewhat incomplete. As a matter of fact, if there is an integration between electric and thermal energy, different performance parameters, such as exergy efficiency, should be analyzed. This would allow a proper weighting for the contribution of each energy flux. Furthermore, previous results ([2,3]) showed that, for a given heat source temperature, the lower the temperature difference between the source and the storage, the higher the performance in terms of η_{rt} are. In other words, if η_{rt} is to be maximized, the HP cycle tends to be as thin as possible, i.e. with the evaporation and condensation temperatures very close, in order to maximize the COP, up to the point where the PTES degenerates in a mere ORC. The ORC alone can only produce electric energy, so it cannot fulfil the PTES role of *storing* electric energy. For reasons that will be clarified in the following sections, similar considerations can also be drawn for the hot reservoir volume, and for the amount of thermal energy which is recovered (and not wasted) from the heat source.
As a matter of fact, if PTES electric size is fixed, the storage volume tends to infinity when η_{rt} is maximized, hence the most efficient TI-PTES tends to have null energy density. The opposite is true for the amount of recovered thermal energy. When η_{rt} is maximized, the heat source exploitation is minimized and the TI-PTES not only degenerates towards an ORC, but it degenerates towards the ORC that have the maximum cycle efficiency allowed by the heat source temperature, which is also the ORC with the minimum net power output, i.e. zero.
Obviously, these extreme configurations should be avoided by constraining variables and by setting minimum values for HP temperature lift and heat source glide, as done in [2,3]. Nonetheless, parameters such as exergy efficiency and energy density, other than the η_{rt}, are needed to fully characterize the proposed application. Since concurrent maximization of these parameters is not achievable in practice, the proper framework to characterize the PTES is the multi-criteria analysis. Therefore, a multi-objective optimization has been performed to fully explore the TI-PTES performance potentialities and limitations.
In this study, a recently proposed TI-PTES configuration, which exploits a low-grade heat source ($T_{src} \leq 80$ °C) and is made up of a vapor compression HTHP and an ORC, is analyzed in respect of three parameters, namely *electric* roundtrip efficiency, energy density and exergy efficiency. The analysis is performed by means of a multi-objective optimization which involves, among the other variables, the HTHP and ORC temperature levels and working fluids.

The main contribution of this paper is in the extensive thermodynamic characterization of a recently proposed PTES configuration, which provides original insights on the performances and limitations of these innovative electric energy storage systems.

2. Methodology

2.1 Cycle architecture

PTES systems are usually composed by a HP, a thermal storage and a thermal engine. In the analysis, a vapor compression heat pump, a two-reservoir sensible heat storage and an ORC are assumed for the HP, the hot reservoir and the thermal engine, respectively. Sensible heat storage is less efficient and dense, if compared to latent heat storage. Despite this, it is still not clear if stable and reliable latent heat storages can be currently deployed in the temperature range of interest (100 °C – 180 °C) [22,23]. In addition, latent heat storage is still an immature technology whose cost turn out to be prohibitive in the current practice. For these reasons, sensible heat storage is selected. Two-reservoir configuration guarantees almost constant charge and discharge profiles at the cost of doubling the storage volume. The selection between two-reservoir and single-reservoir thermal storage is a trade-off between cost and efficiency and can only be solved with a thermo-economic optimization of the system. Such analysis is out of the scope of this paper, so just the most efficient solution between the two is selected.

In addition to basic PTES configuration, also a modified architecture is proposed and investigated. In comparison to basic configuration, both HTHP and ORC are internally regenerated, then two additional heat exchangers are introduced in the system. Again, whether the regeneration should be introduced in the system, is only a matter of thermo-economic analysis. The regenerated configuration outperforms the basic one, but it also entails higher capital expenditures. Since only a thermodynamic assessment is performed here, a final recommendation upon which system is better is not provided, and only relative performance increases between the two configurations are presented.

A graphical representation of the analyzed configurations is reported in Figure 1 (a) and (b) for the basic architecture and the regenerated one, respectively.

Both HTHP and ORC performance is affected by a number of parameters (isentropic efficiencies, heat exchanger approach points, etc.) which are assumed to be constant in the analysis. The numerical values assumed for these parameters are reported in Table 1 and 2 for the HTHP and the ORC, respectively. Some of the listed parameters directly affect the subsystem performances, whereas others are included into the analysis because they represent technical constraints which must be satisfied to provide a realistic representation of the system. Among the latter, $T_{max,hp}$, $p_{min,hp}$ and $p_{min,orc}$ set maximum and minimum values for temperatures and pressures achievable in the system. These limitations stem from the fact that in current HTHP practice the compressor discharge temperature is limited to 180 °C to prevent lubricant oil degradation [24]. Of course, if oil free compressors are used, this limitation does not hold anymore. Despite this, not much higher temperatures may be achieved anyway, since several HTHP working fluids start to show thermal decomposition over 200 °C [18]. Since HTHP compressor discharge temperature is the higher temperature achieved by the whole system, a limitation on this parameter automatically set a limitation on maximum storage and ORC temperatures. As far as $p_{min,hp}$ and $p_{min,orc}$ are concerned, some authors recommend above-atmospheric conditions for obvious reasons [25]. Despite that, a low degree of vacuum can be accepted, especially for small-sized systems where the heat exchanger dimension are moderate [18]. For this reason, 0.5 *bar* is set as the minimum achievable value in both the HTHP evaporator and ORC condenser.

Finally, for the calculation of some performance indicators, such as exergy efficiency, HTHP charge time τ_{hp} in *hours* is needed. Such figure should not be decided a priori, as it should be calculated by considering thermal energy and electric energy availability, and electric energy prices. Given these assumptions, the storage charge/discharge profile is usually optimized to maximize some objective function, which often is the economic revenue (for a similar analysis in the case of battery storage, see [26,27]). Such analysis is out of the scope of the present study, so an arbitrary numeric value equal to 4 *h* is assumed for τ_{hp}. Despite being arbitrary, this value is realistic in the electric storage practice [26,28], as it is essentially related to the shape of the electric energy price daily trend.

Table 1. HTHP technical and operational parameters

$\eta_{is,cmp}$ [-]	$\eta_{el,mot}$ [-]	$PP_{hp,ev}$ [°C]	$PP_{hp,cd}$ [°C]	$PP_{hp,rg}$ [°C]	$T_{hp,max}$ [°C]	$p_{hp,min}$ [bar]	τ_{hp} [h]	$\Delta T_{hp,min}$ [°C]
0.8	0.95	5	5	10	180	0.5	4	20

ORC condensation heat load is assumed to be rejected into environment by means of an air condenser. Therefore, the fan electric consumption is computed and cut out from the gross ORC power output. The fan consumption is a function of the pressure drop across the heat exchanger Δp_{fan} and the fan "efficiency" η_{fan} which accounts for the conversion chain between electric power and mechanical power transmitted to the fluid.

Table 2. ORC technical and operational parameters

$\eta_{is,exp}$ [-]	$\eta_{is,pmp}$ [-]	$\eta_{el,gen/mot}$ [-]	$PP_{orc,ev}$ [°C]	$PP_{orc,cd}$ [°C]	$PP_{orc,rg}$ [°C]	$p_{orc,min}$ [bar]	Δp_{fan} [Pa]	η_{fan} [-]	$T_{air,in}$ [°C]	$T_{air,out}$ [°C]	$\Delta T_{orc,sc}$ [°C]	$\Delta T_{orc,min}$ [°C]
0.85	0.7	0.95	5	10	10	0.5	100	0.6	20	30	5	20

Other relevant modeling assumptions are: pressure drop in heat exchangers are neglected, steady state operation is analyzed, environmental reference temperature T_0 is assumed to be equal to 20 °C and storage thermal losses are considered through a fixed thermal efficiency η_{st} equal to 0.95.

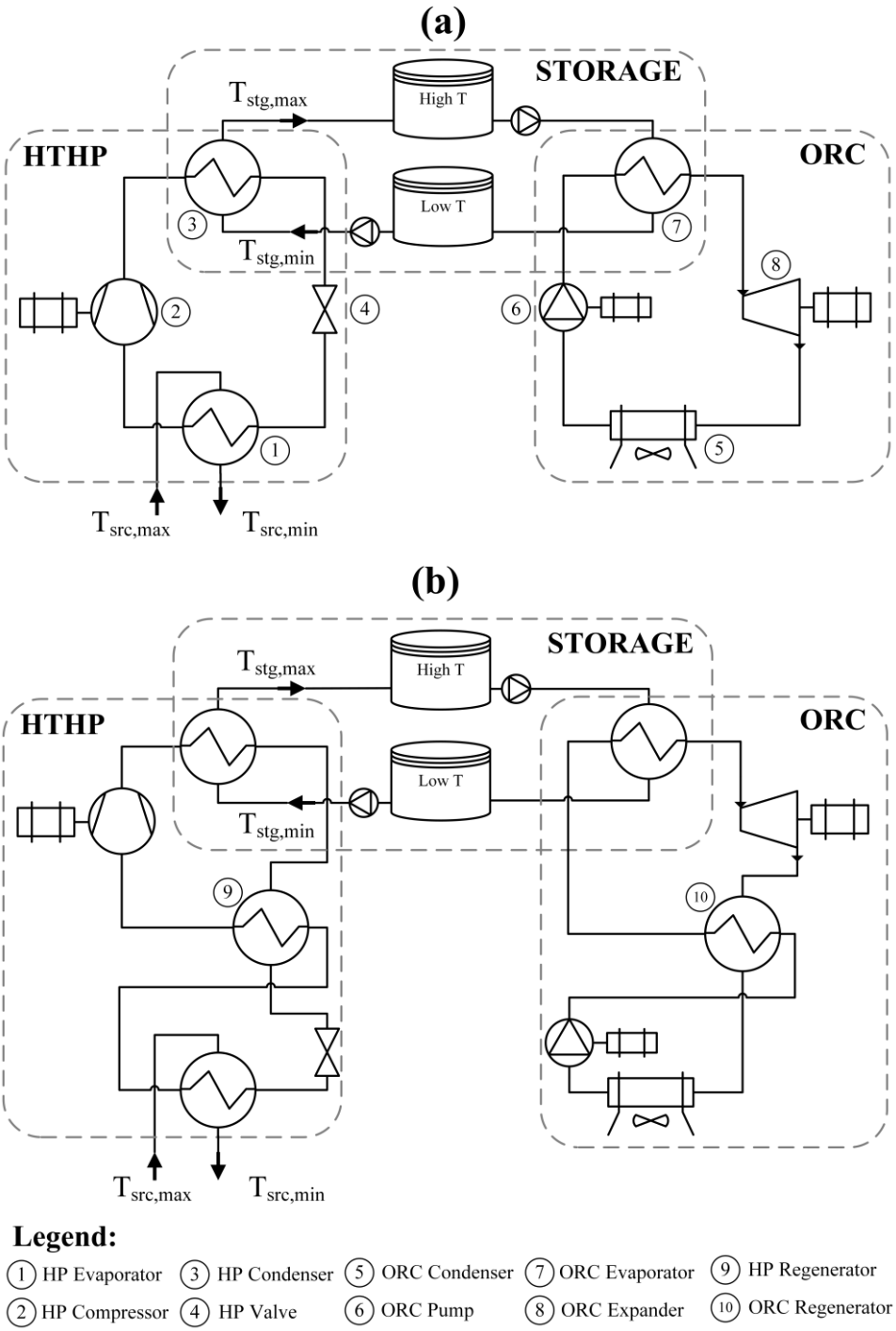

Figure 1. TI-PTES system layout. (a): basic configuration. (b): internally regenerated configuration.

2.2 Performance parameters

Performance of a storage can be measured according to several parameters, but the most important one is the electric-to-electric efficiency (or round-trip efficiency, or back-work ratio) η_{rt}. For traditional electric storage technologies (i.e. batteries, flywheels, PHES, etc.) η_{rt} coincides also with first-law and second-law efficiencies, which is not the case for hybrid storage technologies like the TI-PTES. For these systems, η_{rt} is still important, because it is related with the economic revenue of the storage and its operating costs. Nonetheless, since also some thermal energy is absorbed, a different formulation of the efficiency may be considered. It could seem natural to directly select classical exergy efficiency formulation, but this would imply that the thermal energy is exactly available when needed. This is certainly possible, but it would require either to produce the thermal

energy with fossil fuels or electric energy (which is a nonsense), or to store the thermal energy provided by the heat source to make it available on request. In this case, the heat could certainly be produced with solar collectors or by exploiting geothermal or waste heat sources, but at least an additional thermal storage, if not a solar collector field, should be added to the systems in Figure 1 (a) and (b). Furthermore, a fair comparison between the TI-PTES and other more traditional storage technologies is based on the fact that the heat source thermal energy is considered as "readily available", which is actually a way to say "for free" (or at least "really cheap"). This not certainly apply to the case in which the heat is provided by a geothermal well or by a field of solar collectors, which are both quite expensive heat sources. This does not exclude the fact that such applications might be very interesting, but a tecno-economic assessment would be mandatory in these cases, since the economic viability of such system would be the major concern.
In short, by choosing the straightforward exergy efficiency formulation, the perfect contemporaneity between thermal and electric energy availabilities is implicitly assumed. This can be difficultly assumed without either adding some pieces of equipment, or by including into the analysis an economic assessment.
To get rid of the contemporaneity hypothesis, it must be accepted that some losses will occur on the heat source side. To do so, it is assumed that the heat is provided for τ_{src} *hours*, but it is exploited only for τ_{hp} *hours*. To conservatively assess TI-PTES performances, τ_{src} is assumed to be equal to 24 *h*, while τ_{hp} is equal to 4 *h*, as reported in Table 1. In other words, the TI-PTES exploits the heat source for one sixth of the total available time.
To limit the analysis to the systems reported in Figure 1 (a) and (b), while also providing results that can be used for a fair comparison between TI-PTES and other storage technologies, the heat source is assumed to be waste heat. As already pointed out, this is the only case in which the provided amount of thermal energy could be considered as "readily available", i.e. "for free".
Based on the energy fluxes between TI-PTES subsystems reported on Figure 2, the metrics to measure PTES performances are defined as follows. The first parameter is the roundtrip efficiency η_{rt} which accounts for the ratio between the absorbed and returned amounts of *electric* energy by the HTHP and the ORC, respectively. Based on Figure 2, and considering previous analysis from [2,3], the following holds (Eq. 1):

$$\eta_{rt} = \frac{L_{hp}}{L_{orc}} = COP \cdot \eta_{orc} \cdot \eta_{stg} \tag{1}$$

By considering Figures 1 (a) and (b) layouts and commonly accepted definitions for *COP* and η_{orc}, it can be written (Eq. 2):

$$COP = \frac{\Delta h_{hp,cd}}{\Delta h_{hp,cmp}/\eta_{el,mot}} \tag{2}$$

Where $\Delta h_{hp,cmp}$ and $\Delta h_{hp,cd}$ are the enthalpy differences across the HTHP compressor and condenser, respectively. As regards to η_{orc} (Eq. 3):

$$\eta_{orc} = \frac{\Delta h_{orc,exp} \cdot \eta_{el,gen} - \frac{\Delta h_{orc,pmp}}{\eta_{el,mot}} - \Delta h_{orc,cd} \cdot \frac{\Delta p_{fan}}{cp_{air} \cdot \rho_{air} \cdot \eta_{fan} \cdot (T_{air,out} - T_{air,in})}}{\Delta h_{orc,ev}} \tag{3}$$

where $\Delta h_{orc,exp}$, $\Delta h_{orc,pmp}$, $\Delta h_{orc,cd}$ and $\Delta h_{orc,ev}$ are the enthalpy differences across the ORC expander, pump, condenser and evaporator, respectively. cp_{air} and ρ_{air} are the specific heat and the density of air averaged between $T_{air,out}$ and $T_{air,in}$.
The exergy efficiency ψ_{ut} can be defined as in Eq. 4:

$$\psi_{ut} = \frac{Ex_{orc}}{Ex_{src} + Ex_{hp}} \tag{4}$$

where Ex_{orc}, Ex_{src} and Ex_{hp} are the exergy amounts which are absorbed, or delivered, by ORC, heat source and HTHP, respectively. By applying energy balances on the subsystems, COP definition and Eq. 1, Ex_{orc}, Ex_{src} and Ex_{hp} can be rewritten as in Eq. 5 – 7:

$$Ex_{orc} = L_{orc} = \eta_{rt} \cdot L_{hp} = \eta_{rt} \cdot Ex_{hp} \tag{5}$$

$$Ex_{src} = \dot{m}_{src} cp_{src} \cdot \left[\Delta T_0 - T_0 \cdot ln\left(\frac{T_{src,max}}{T_0}\right)\right] \cdot \tau_{src} \quad (6)$$

where, T_0 = 20 °C is the reference temperature, $\Delta T_0 = T_{src,max} - T_0$ is the maximum potential cooling of the heat source and $\dot{m}_{src}$ and cp_{src} are the heat source fluid mass flow rate and specific heat at constant pressure, averaged between the heat source maximum and minimum temperatures $T_{src,max}$ and $T_{src,min}$. Finally, for Ex_{hp} it can be written:

$$Ex_{hp} = \frac{\dot{Q}_{src}}{COP-1} \cdot \tau_{hp} = \frac{\dot{m}_{src} cp_{src} \Delta T_{src}}{COP-1} \cdot \tau_{hp} \quad (7)$$

where $\Delta T_{src} = T_{src,max} - T_{src,min}$. By substituting Eq. 5, 6 and 7 in Eq 4, the following can be achieved (Eq. 8):

$$\psi_{ut} = \frac{\eta_{rt} \cdot \Delta T_{src}}{(COP-1) \cdot \left[\Delta T_0 - T_0 \cdot ln\left(\frac{T_{src,max}}{T_0}\right)\right] \cdot \frac{\tau_{src}}{\tau_{hp}} + \Delta T_{src}} \quad (8)$$

The last parameter to measure system performance is the energy density ρ_{en} measured in kWh/m^3. ρ_{en} is useful to account for relative dimension of the system. For the same reason why it is important to include ψ_{ut} in the analysis, ρ_{en} can provide useful insights on the implicit trade-offs that must be accepted in order to maximize η_{rt}. Storage maximum and minimum temperatures $T_{stg,max}$ and $T_{stg,min}$ are comprised between HTHP condensation and evaporation temperature levels, as the storage is charged by the HP condenser. In a two-reservoir sensible heat storage, the energy per unit of fluid volume is inversely proportional to the temperature difference between the two reservoir, which is $\Delta T_{stg} = T_{stg,max} - T_{stg,min}$. Therefore, if ρ_{en} is to be maximized, also ΔT_{stg} should be maximized. However, ΔT_{stg} is limited by the HTHP lift, which tends to be minimized in order to maximize η_{rt}. this means that for a TI-PTES system η_{rt} and ρ_{en} are competing objectives. Since TI-PTES is a stationary storage, ρ_{en} is certainly a secondary parameter but a very low value of ρ_{en} entails very large storage volumes, and this can make system costs grow. Furthermore, a very large thermal storage has also a very large surface area and this entails larger thermal losses, which should be avoided to maximize PTES performance.

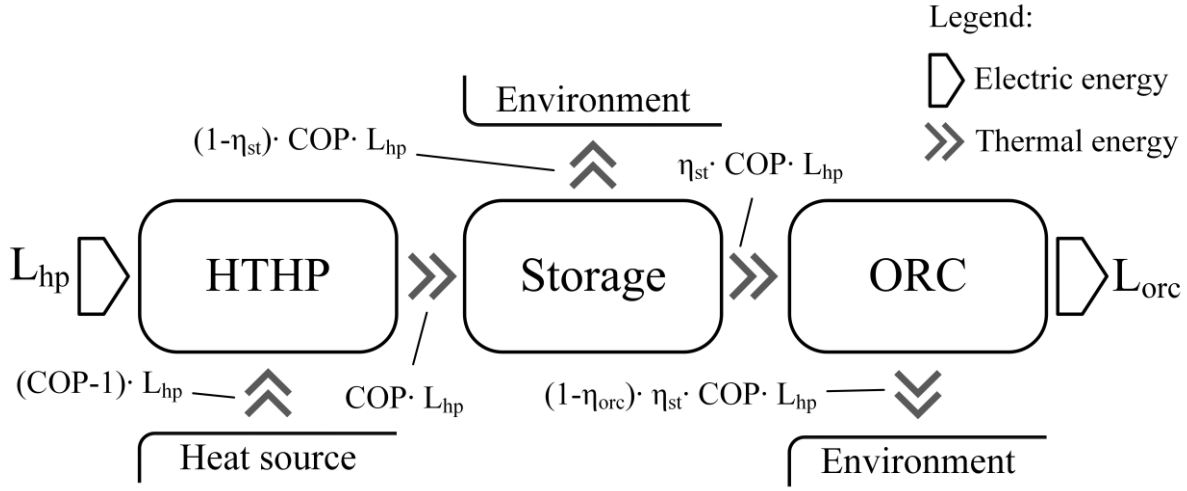

Figure 2. Energy fluxes between TI-PTES subsystems.

In the present analysis, ρ_{en} is defined as the ratio between the share of the stored energy that can be effectively converted into electric energy, and the storage volume in m^3. Therefore, it can be written as in Eq. 9:

$$\rho_{en} = \eta_{orc} \cdot \rho_{stg} cp_{stg} \Delta T_{stg} / 3600 \quad (9)$$

where ρ_{stg} and cp_{stg} are the density and the constant pressure specific heat of thermal storage fluid. The storage is assumed to use slightly pressurized water, but thermal oil could be used as well, if cheaper alternatives are to be pursued. In this case, the energy density numerical value would change, but the general trend of ρ_{en} and its trade-off with η_{rt} would maintain the same physical meaning. It is worth mentioning that since a double reservoir solution is used, a ½ factor could be multiplied to ρ_{en}, if in Eq. 9 the total volume, and not the active

volume, is considered. Like said before, this would change the numerical value of ρ_{en}, but not the physical meaning of its trade-off with η_{rt}.

2.3 Optimization problem

To extensively explore the trade-off between η_{rt}, ψ_{ut} and ρ_{en}, a multi-objective optimization approach is followed. The TI-PTES is designed in a flexible way, such that its design parameters can be adjusted to promote one of the listed metrics. In other words, the TI-PTES design is performed through an optimization problem, which have HTHP, ORC and storage design parameters as variables. In order to give a realistic representation of the physical system some constraints must be enforced. They represents physical and technical limitations like heat exchanger pinch points, minimum achievable pressure in HTHP evaporator and ORC condenser, etc. For the TI-PTES non-regenerated configuration reported in Figure 1 (a), optimization variables are:

- $T_{src,min}$, minimum cooling temperature achieved by the source while providing heat to the HTHP;
- $T_{hp,ev}$, $T_{hp,cd}$, $\Delta T_{hp,sh}$ and $\Delta T_{hp,sc}$, HTHP evaporation and condensation temperatures, as well as superheating and subcooling at the evaporator and condenser exit, respectively;
- $T_{orc,ev}$, $T_{orc,cd}$ and $\Delta T_{orc,sh}$, ORC evaporation and condensation temperatures, as well as superheating at the evaporator exit;
- $T_{stg,max}$ and $T_{stg,min}$, storage maximum and minimum temperature.

If the internal regeneration is introduced, an additional optimization variable must be used:

- $\Delta T_{orc,rg}$, temperature difference between the inlet and outlet of the hot side of the ORC regenerator.

Although HPs and ORCs are quite "symmetrical" systems, such that some authors investigated reversible configurations [29–31], the HTHP and ORC modelling proposed here is not perfectly symmetrical. Subcooling and regeneration can be managed differently from the optimization point of view in HTHPs and in ORCs. In particular, $\Delta T_{orc,sc}$ it is assumed, and not optimized, because it is a necessary ORC feature to prevent pump cavitation, but it is usually minimized because it does not have any positive effects on the efficiency. Likewise, there is no need to optimize $\Delta T_{hp,rg}$ as the internal regeneration in HTHP is used to provide the superheating at the evaporator exit. Therefore, the influential variable is still $\Delta T_{hp,sh}$, from which $\Delta T_{hp,rg}$ can be readily calculated through the HTHP regenerator energy balance.

As far as the constraints are concerned, in non-regenerated configuration the problem has 20 bound constraints, 8 linear constraints and 9 non-linear constraints. In regenerated configuration the problem has 22 bound constraints, 8 linear constraints and 13 non-linear constraints. Due to the high number of constraints, the complete list is reported in Appendix A.

The constraints enforce some relations that must be respected due to the physical phenomena that characterize the PTES system. A large part of both linear and non-linear constraints is dedicated to the observance of heat exchangers pinch points. Two non-linear constraints guarantee that the HTHP has an entirely dry compression and that the ORC expansion ends with a vapor quality higher than 0.85. Some bound constraints guarantee that neither maximum allowable temperatures, nor minimum allowable pressures are exceeded, while some other enforce subcritical working conditions to HTHP and ORC cycles.

If only one parameter among η_{rt}, ψ_{ut} and ρ_{en} is to be maximized, the resulting optimization problem has a scalar objective function, and it can be potentially solved with any non-linear programming technique. In the analysis a SQP algorithm has been used, as implemented in [32]. Even though the problem is not smooth in theory, as reported in Appendix A, where it is shown that some constraints are based on $min(\cdot)$ and $max(\cdot)$ functions, in practice the problem is sufficiently smooth to be solved with an algorithm based on derivatives. The same can be said for the use of CoolProp [33] and REFPROP [34] to evaluate HTHP and ORC fluid thermophysical properties. Each evaluation is based on the numerical solution of the fluid equation of state and this make the objective function a black box, which can be numerically evaluated, but does not have derivatives. Nevertheless, the numerical evaluation of gradients and hessians is possible due to the general smoothness of thermophysical properties which makes the problem solvable with gradient-based approaches.

The design optimization problem is highly non-linear, without an analytical representation and non-convex, most likely. To try to prevent the optimizer from converging on local minima, a multi-start strategy is adopted, and each optimization is repeated 10 times, from different initial points. A higher number of starting points do not significantly improve the solution, then the optima found through this procedure have been considered as global optima.

When the optimal trade-off between η_{rt}, ψ_{ut} and ρ_{en} is to be investigated, the objective function becomes a vector function. In this case, a common approach is to "scalarize" the problem, by converting it back to a single objective problem. Several scalarization techniques have been proposed in literature, and that used here is the

scalarizing approach based on reference points proposed by Wierzbicki [35] and reported also more recently in [36]. The resulting problem has the same set of constraints of the single objective problem, reported in Appendix A, and it can be solved with the same algorithmic approach, but it has a modified objective function, as follows in Eq. 10:

$$f_{sf} = \max_i \left[f_i(\boldsymbol{x}) - f_{i,ref} \right] + \alpha \sum_i \left[f_i(\boldsymbol{x}) - f_{i,ref} \right] \quad (10)$$

where $\boldsymbol{f}(\boldsymbol{x}) = [\eta_{rt}(\boldsymbol{x}), \psi_{ut}(\boldsymbol{x}), \rho_{en}(\boldsymbol{x})]$ is the objective vector, $\boldsymbol{f}_{ref} = [\bar{\eta}_{rt}, \bar{\psi}_{ut}, \bar{\rho}_{en}]$ is an arbitrary point in the objective space to be achieved and $\alpha = 10^{-4}$ is an arbitrary constant, often called augmentation coefficient. α multiplies the augmentation term of f_{obj}, and its purpose is to rule out weakly-Pareto points. By minimizing f_{sf}, the reference point gets "projected" onto the Pareto front and the resulting optimal $\boldsymbol{x}$ yields one point of the Pareto front. By varying $\boldsymbol{f}_{ref}$, the Pareto front can be explored and the optimal trade-off between η_{rt}, ψ_{ut} and ρ_{en} investigated.

2.4 Working fluid Pair selection

A good share of research activities on HTHP and ORC is dedicated to the choice of best suited working fluid, as demonstrated also by [16,18]. Even in the case of TI-PTES, the choice of working fluid pair is an open problem. In the case of latent heat storage, some recommendations can be found in [2,3], but the use of a sensible heat storage brings up new challenges from the point of view of HTHP and ORC thermal profiles integration, and the working fluid pair must be re-evaluated for this new architecture.

The working fluid pairs could be optimized together with the rest of the PTES system, but this would lead to a mixed-integer non-linear problem, with an increased complexity. To avoid this, a representative subset of working fluids is selected and exhaustively investigated by iteratively optimizing all the possible couples. The investigated fluids are selected among a pool of natural and artificial refrigerants which are promising for both HTHPs and low temperature ORCs. Based on previous researches [16,18,37], the investigated fluids are: Cyclo-Pentane, Pentane, R1233zd(E), R1224yd(Z), R245fa, R1336mzz(Z), R365mfc and R1234ze(Z).

All these fluids show good performance when used for HTHP and ORC in the investigated temperature range. Besides that, they all have very low GWP (less than 5), except for R245fa and R365mfc, which have GWP equal to 804 and 1030 [16,38]. Even if R245fa and R365mfc have a non-negligible environmental impact, their use is still allowed. Therefore, most of the commercial HTHP systems propose the R245fa as working fluid [16,17]. All the selected fluids can be used in HTHP and ORC systems from all the technical points of view (material compatibility, thermal decomposition and safety standard), as discussed in [18]. Whenever possible, the thermophysical properties of the fluids are evaluated using the software CoolProp v. 6.2.0 [33]. Otherwise, for the fluids still not implemented in CoolProp, i.e. R1336mzz(Z) and R1224yd(Z), REFPROP v. 10.0 [34] is used.

3. Results and discussion

3.1 Working fluid pair selection

The exhaustive investigation of all the possible working fluid pairs leads to identify the most performant fluid arrangements in terms of the three parameters η_{rt}, ψ_{ut} and ρ_{en} for both the regenerated and non-regenerated layouts. For the sake of brevity, the complete set of results is reported in Table B1 and B2 of Appendix B, while the most performing couples are reported in Table 3.

As resulted, Cyclopentane is the recommended fluid to achieve high efficiency. If η_{rt} is to be maximized, Cyclopentane is always recommended for the HTHP, for both regenerated and non-regenerated configuration. This is supported also by previous studies, which identify Cyclopentane as one of the most efficient fluid for the use in HTHP in the investigated temperature range [18]. As can be noted from Tables 3, B1 and B2, ρ_{en} is not influenced by HTHP fluid choice. This stems from the fact that ρ_{en} is defined such that none of the HTHP-related variables play an explicit role on its computation (see Eq. 9). Despite this, every optimization problem is solved by considering the same set of constraints, which do take HTHP-related variables into account. Therefore, ρ_{en} can be influenced, at least in theory, by the HTHP fluid choice. However, this does not happen in the practice. A possible reason for this is that none of HTHP fluids reaches the minimum allowed pressure at a temperature that poses any limitation on the storage temperature difference ΔT_{stg}. This is relevant because ΔT_{stg} must be maximized in order to maximize ρ_{en}, as previously discussed. Likewise, none of the HTHP fluids have a critical temperature low enough to pose a higher bound on ΔT_{stg}. This is because, within certain limits, a lower T_{crit} can be compensated by modifying the rest of the HTHP cycle. In conclusion, ρ_{en} is limited by

HTHP specifications which does not depend on the fluid. This is an indirect confirmation that the investigated fluids are well suited to be integrated in the considered temperature range.

Table 3. Fluid selection results. Best achieved values and best working fluid pairs in respect to η_{rt}, ψ_{ut} and ρ_{en}. Relative percentage increments due to internal regeneration introduction are also reported.

Layout:	Non-regenerated			Regenerated		
Parameter:	η_{rt} [-]	ψ_{ut} [-]	ρ_{en} [kWh/m^3]	η_{rt} [-]	ψ_{ut} [-]	ρ_{en} [kWh/m^3]
HTHP fluid:	Cyclopentane	Cyclopentane	–	Cyclopentane	R1336mzz(Z)	–
ORC fluid:	Cyclopentane	Cyclopentane	R1234ze(Z)	R365mfc	R1336mzz(Z)	R1336mzz(Z)
Value:	0.608	0.184	13.074	0.647	0.212	17.722
Increment %:	–	–	–	6.414	15.217	35.551

When regenerated layout is considered, R1336mzz(Z) is one of the best fluids, as it maximizes ψ_{ut} and ρ_{en} and, as shown in Table B2, it achieves also a quite high η_{rt}. By comparing Table B1 and B2, it is clear that the R1336mzz(Z) is a performant fluid only if used in conjunction with internal regeneration. In non-regenerated case R1336mzz(Z) is one of the worst fluids, together with R1224yd(Z) and R245fa. This is most likely due to the high slope of saturated vapor boundary line in *T-s* plane, which forces HTHP cycle to use high superheating after the evaporation to ensure a totally dry compression. Without the regeneration, which decouples superheating (i.e. $\Delta T_{hp,sh}$) from heat source temperatures, the resulting HTHP cycle is forced to have higher temperature lifts, and thus lower COPs. This happens because both evaporation and superheating must occur at lower temperature, being bounded by the heat source. Conversely, when regeneration is adopted, superheating can be increased without being limited by heat source temperatures and without affecting evaporation temperature, within certain limits.

Compared to Cyclopentane, R1336mzz(Z) has lower electric-to-electric efficiency but it could still be the preferred alternative, for an actual TI-PTES implementation, depending on the compressor technology that is used. R1336mzz(Z) has much higher volumetric heating capacity than Cyclopentane [16,18], which leads to much lower volumetric flowrates, as the thermal capacity of the system is fixed. Low volumetric flow rates are required in case of volumetric compressors, while this limitation is typically less severe for centrifugal compressors.

Similar considerations might also be drawn for ORC expander technology, but the value assumed for $\eta_{is,exp}$ (Table 2) are more consistent with dynamic expanders.

In the practice, working fluid choice would be based on a much broader reasoning than that provided by the thermodynamic analysis conducted here. A detailed techno-economic analysis cannot be avoided in this context. Therefore, when comparing two fluids, it is worth remembering that their differences are more than those analyzed here.

In Table 3 the results concerning the performance increment due to regeneration introduction are reported. Regeneration is beneficial for all the three monitored performance parameters. However, the regeneration is not very effective in respect to η_{rt}, while for ψ_{ut} and ρ_{en} higher increments are achieved. On the other hand, high η_{rt} relative increments (over 10%) are achieved in some specific cases, like for R1336mzz(Z), R365mfc and Pentane. The same fluids are also those that show the highest ρ_{en} increments, thus suggesting that a major share of the η_{rt} increase is due to increments in η_{orc} (that affects both η_{rt} and ρ_{en}).

Regeneration is very effective in regards of ρ_{en}, both by comparing regenerated and non-regenerated best values and by comparing single fluid values. This stems from the fact that the regeneration boosts η_{orc}, by making it less sensitive to storage temperature profile. In other words, regeneration allows ΔT_{stg} to be increased, without η_{orc} being too much compromised.

By comparing the increease in η_{rt}, ψ_{ut} and ρ_{en} reported in Table B3 with the slopes of the saturated vapor phase boundary line reported in Figure B1, it can be observed that there is a strong correlation between regeneration effectiveness and saturated vapor line slope. In other words, the more the saturation line is inclined, the higher is the regeneration benefit. A partial exception is Cyclopentane, whose saturation line is relevantly inclined if the whole *T-s* plane is considered. Despite this, the Cyclopentane is the fluid that receives less benefits from regeneration. This is because, differently from the other investigated fluids, Cyclopentane has the critical temperature much higher than the investigated PTES temperature levels. Within the temperatures investigated here, Cyclopentane has rather vertical saturated vapor line, so it locally behaves like an isentropic fluid (i.e. like R1234ze(Z)) and not like a dry fluid, as it is.

These last considerations and the values reported in Table B3 for η_{rt} and ρ_{en} increments suggest that most of performance increases are related to the ORC regeneration, and not the HTHP regeneration. The reason why

this happens will be clarified later, when some examples of HTHP and ORC cycles will be presented. It can be anticipated that, since the configurations that maximize η_{rt} are also those which work with the lowest possible HTHP temperature lift, the resulting HP cycle is already very "thin", and the regeneration cannot help in making this cycle even thinner. This is also reflected in the mathematical model, where the HP lift is bounded to avoid very low temperature lifts. This might make HTHP operation unstable, since little temperature variations might lead to huge COP variations, as the mathematical relation between COP and Temperature lift is very steep when this last is approaching zero.
Similar considerations may be drawn for the case which maximizes ρ_{en}. In this case, most of HTHP performance is traded in favor of the ORC, and this means that HP lift tends to be large. As far as the regeneration is concerned, since η_{orc} is to be maximized, HTHP condensation already works at its maximum operational temperature $T_{hp,max}$, then the regeneration cannot further increase this value. Therefore, HTHP regeneration alone would not be able increase ρ_{en}.
A different situation can be observed in Table B3 for ψ_{ut} increments. In this case, the additional degree of freedom provided to the HTHP cycle by regeneration makes a difference, and ψ_{ut} increments depend on the HTHP operational conditions and selected fluid. The highest increases are still registered by those fluids whose saturation line is steeper, i.e. R1336mzz(Z), R365mfc, R1224yd(Z), Pentane, and R245fa, because these fluids might require a superheating degree at the evaporator exit higher than usual to ensure dry compression, as discussed before. Nonetheless, also "isentropic" fluids like Cyclopentane and R1234ze(Z) are affected by relevant increments (roughly between 15% and 20%), often comparable with the other abovementioned fluids.
Now that the "extreme" TI-PTES configuration have been investigated both in regenerated and non-regenerated cases, the analysis can be narrowed down to the fluid pairs that perform the best. Since from Table 3 no clear winners can be selected, the working fluid choice is arbitrary and it is based on the relative weight that are assigned to η_{rt}, ψ_{ut} and ρ_{en}. Since the trade-off between the three is to be investigated, balanced fluid pairs are here preferred, not to penalize from the beginning one parameter over another.
A mathematical way to translate this is to assign to each fluid pair a score, based on the weighted sum of the values of η_{rt}, ψ_{ut} and ρ_{en}. To get rid of differences in scale, the values reported in Tables B1 and B2 are normalized, by using their maximum values, reported in Table 3. Since no preference among the parameters is expressed here, the weights are all the same (so any arbitrary value can be chosen). The score SC can be calculated as in Eq. 11:

$$SC = W_1 \frac{\eta_{rt}}{\eta_{rt}^{max}} + W_2 \frac{\psi_{ut}}{\psi_{ut}^{max}} + W_3 \frac{\rho_{en}}{\rho_{en}^{max}} \quad (11)$$

Where W_i are the weights.
The outcome of this calculation led to identify the pair Cyclopentane – Cyclopentane as recommended for non-regenerated case, and the pair R1336mzz(Z) – R1336mzz(Z) as recommended for regenerated case.
In Figure 3 (a – c) non-regenerated configurations which maximize η_{rt}, ψ_{ut} and ρ_{en} for the pair Cyclopentane – Cyclopentane pair are reported. Similarly, in Figure 3 (d – f) regenerated configurations for the pair R1336mzz(Z) – R1336mzz(Z) are reported. In Figure 3, many of already commented TI-PTES features can be confirmed. The configurations that maximize η_{rt} (a and d) show minimum HTHP temperature lift. As expected, HP cycle is as thin as possible to maximize the COP, to the detriment of the ORC performance. Therefore, COP is preferred over η_{orc}, from the roundtrip efficiency point of view. This is not because η_{rt} does not depend on η_{orc}, but because relative increments of COP are much higher than those of η_{orc}, in the investigated temperature levels. For the very same reason, as already discussed, in the case in which a lower limit for HTHP lift is not given, the TI-PTES degenerates towards an ORC.
Conversely, the configurations which maximize ψ_{ut} (b and e) have maximum HTHP lift. In this case, HTHP condensation and evaporation are bounded by $T_{hp,max}$ and environmental temperature T_0, respectively. Maximum lifts allow the maximum recovering of thermal energy from heat source. Anyway, since in ψ_{ut} mathematical expression η_{rt} is also present (Eq. 8), to counterbalance the loss of COP from HTHP side, η_{orc} must be maximized. Accordingly, ORC cycle has the maximum temperature difference between evaporation and condensation, to achieve maximum η_{orc}. In both regenerated and non-regenerated cases, ORC is limited upward by HTHP condensation temperature profile, and downward by T_0.

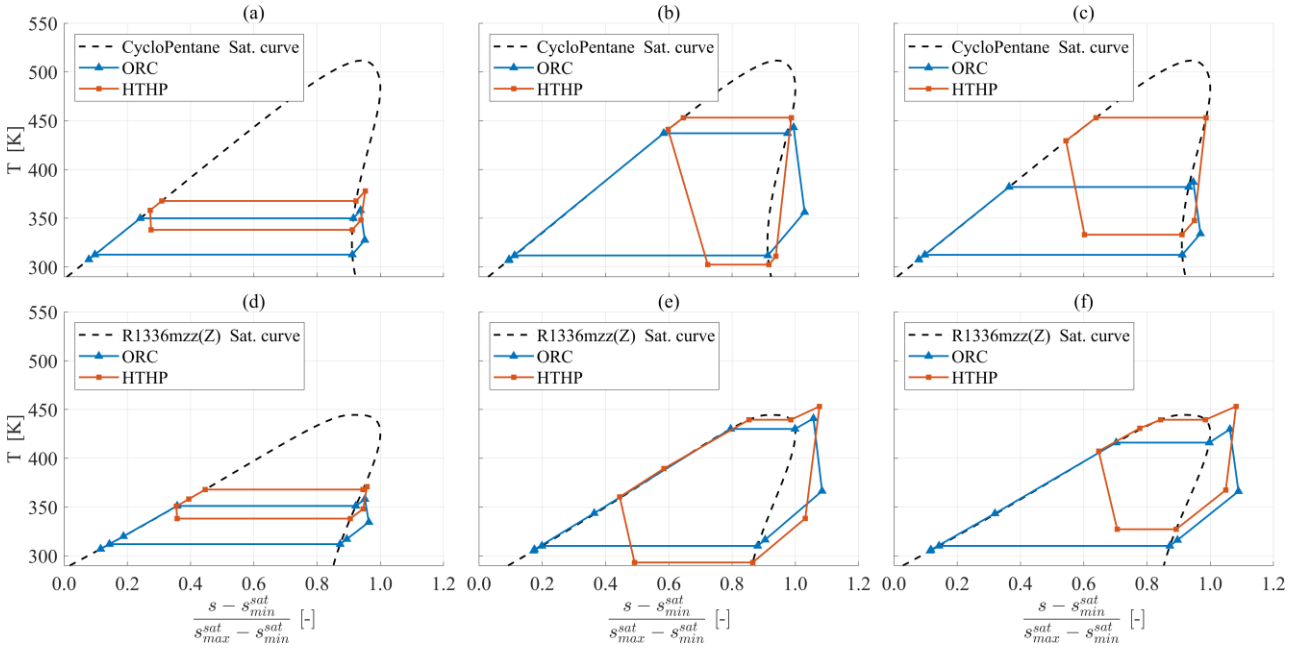

Figure 3. TI-PTES arrangement of HTHP and ORC thermodynamic cycles. (a – c): Non-regenerated layout. (d – f): Regenerated layout. On the x-axis $s_{min}^{sat} = s(T_{min}^{sat}; x = 1)$ and s_{max}^{sat} is the maximum of the entropy achieved over the whole saturation line for $T_{sat} \geq T_{min}^{sat}$., where $T_{min}^{sat} = 290\ K$. (a and d): η_{rt} being maximized; (b and e): ψ_{ut} being maximized; (c and f): ρ_{en} being maximized.

Finally, for the configuration which maximize ρ_{en}, reported in Figure 3 (c and f), it can be seen how the HTHP highest temperature is set at its maximum ($T_{hp,max}$), to maximize $T_{stg,max}$ and thus ΔT_{stg}. Conversely, ORC evaporation temperature it is not maximized, as previously done for the case of ψ_{ut}. This happens because there is a trade-off between $T_{orc,ev}$, which should be increased for increasing η_{orc}, and $T_{stg,min}$, which should be minimized to increase ΔT_{stg} and optimization algorithm finds the optimal trade-off between the two.
In this context, the value of $T_{hp,ev}$ has little influence, so an evaporation temperature that allows the condensation reaches $T_{hp,max}$ at the compressor exit is selected. This is the fundamental feature of the HTHP cycle from the ρ_{en} point of view, so the cycle is modified accordingly to guarantee that.
For the maximization of ψ_{ut}, ORC regeneration allows a certain decoupling between minimum storage temperature $T_{stg,min}$ and ORC evaporation temperature. As a result, the evaporation temperature level can be increased, thus increasing also η_{orc}, while $T_{stg,min}$ remains low.
Once the two working fluid pairs have been selected, the trade-off between η_{rt}, ψ_{ut} and ρ_{en} can be fully explored. Before doing that, some preliminary conclusions can be drawn:

- As reported in Table 3, for the non-regenerated architecture, values around 0.6, 0.18 and 13 kWh/m^3 can be achieved for η_{rt}, ψ_{ut} and ρ_{en}. Conversely, for the regenerated architecture values around 0.65, 0.21 and 18 kWh/m^3 can be achieved for η_{rt}, ψ_{ut} and ρ_{en}. Noticeably, those values cannot be achieved with the same layout as the three objectives are competing one among each other. Therefore, a trade-off solution must be searched;
- Regeneration can be very effective in increasing the PTES performance, depending on the monitored parameter: ρ_{en} showed the best relative increase, equal to around 35%, followed by ψ_{ut}, which showed a relative increase around 15%. η_{rt} resulted as the least affected parameters by the regeneration, with a relative increase around 6.5%. This difference lies in the fact that the cycle architectures which maximize η_{rt} and ψ_{ut} have already reached the limitations imposed by the model (i.e. maximum and minimum temperature levels). Therefore, the introduction of additional degrees of freedom is not very effective. This is not the case of ρ_{en} in which the required trade-off between storage and ORC evaporation temperature profiles is relaxed by the additional degree of freedom provided by the regeneration;
- Results showed that the regeneration on the ORC side is more effective than that on the HTHP side. This is suggested by Table B3 where it is shown that relative increments related to η_{rt} and ρ_{en} do not depend on the HTHP fluid choice;

- If working fluid pairs that perform well on each figure of merit are to be selected, for non-regenerated layout Cyclopentane should be used, for both HTHP and ORC, while for regenerated layout, the same can be said for R1336mzz(Z).

3.2 Multi-objective optimization results

The investigation of optimal trade-off between η_{rt}, ψ_{ut} and ρ_{en} is performed by solving the optimization problem with objective function reported in Eq. 10, which is subjected to the constraints reported in Appendix A. Each optimization gives the coordinates of a Pareto front point, which is the "projection" onto the front of reference point specified in Eq. 10. By moving the reference point, the entire Pareto front can be explored by sampling new points.

Reference points specification is arbitrary and here a regularly spaced grid of points covering all the interesting combinations among η_{rt}, ψ_{ut} and ρ_{en} is used. The range of variations covered by reference points is based on the maximum and the minimum values of η_{rt}, ψ_{ut} and ρ_{en} achieved with the three single objective optimizations. In other words, to construct the reference point grid, the maximum and the minimum values of the pay-off table reported in Table 4 are used. These η_{rt}, ψ_{ut} and ρ_{en} values are those characterizing the configurations previously reported in Figure 3 (a – f).

Table 4. Pay-off table for the configurations maximizing η_{rt}, ψ_{ut} and ρ_{en}, respectively. Related thermodynamic cycles in Figure 3 are reported. Maximum and minimum values for each parameter are underlined in the table.

Maximized	Non-regenerated				Regenerated			
Parameter:	η_{rt} [-]	ψ_{ut} [-]	ρ_{en} [kWh/m^3]	Figure 3:	η_{rt} [-]	ψ_{ut} [-]	ρ_{en} [kWh/m^3]	Figure 3:
η_{rt} [-]	<u>0.608</u>	<u>0.022</u>	<u>0.776</u>	(a)	<u>0.621</u>	<u>0.023</u>	<u>0.818</u>	(d)
ψ_{ut} [-]	<u>0.250</u>	<u>0.184</u>	2.305	(b)	0.335	<u>0.212</u>	13.983	(e)
ρ_{en} [kWh/m^3]	0.256	0.058	<u>11.552</u>	(c)	<u>0.279</u>	0.130	<u>17.722</u>	(f)

Once that a satisfactory representation of Pareto front has been built, there is the need for a criterium to choose, among all the non-dominated solutions, the one that satisfy an arbitrary order of preference among the objectives (i.e. η_{rt}, ψ_{ut} and ρ_{en}). This order of preference, which is no more than a hierarchy of importance between objectives, is usually specified by means of weights, which reflect Decision Maker (DM) preferences. The decision-making criterium assumed here is the well-known TOPSIS [39], which is one of the most common criterium and it is often used in the energy field [40].

For the sake of brevity, only three weight sets $W_{1\text{-}3}$ are investigated (Eq. 12):

$$\begin{cases} W_1 = [1/3;\ 1/3;\ 1/3] \\ W_2 = [1/2;\ 1/2;\ 0] \\ W_3 = [1/2;\ 0;\ 1/2] \end{cases} \tag{12}$$

As can be seen, W_1 specifies the case in which all the three parameters are equally important, while W_2 and W_3 specify two case in which only two parameters are important, while the third is disregarded. In this last case, only the trade-off between two parameters is considered, and the third parameter is left to be chosen accordingly.

W_2 represents the case in which energy density is not considered a problem, according to the point of view for which energy density is a secondary feature for a static storage system. Conversely, W_3 represents the case in which ψ_{ut} is not considered as important, if compared to the efficient use of *electric* energy inputs (i.e. η_{rt}) and energy density. In other words, this is the case in which the heat provided by the heat source is considered not valuable, from both economic thermodynamic point of views. The case in which η_{rt} is disregarded is not investigated as it is considered of no practical interest.

The Pareto points, and the three configurations which are chosen by specifying $W_{1\text{-}3}$, are reported in Figure 4 (a) for the non-regenerated layout and in Figure 5 (a) for the regenerated one. Conversely, in Figure 4 (b) and 5 (b) the ratios between the achieved η_{rt}, ψ_{ut} and ρ_{en} and their respective ideal values, i.e. maximum values reported in Table 4, are reported for non-regenerated and regenerated layout, respectively.

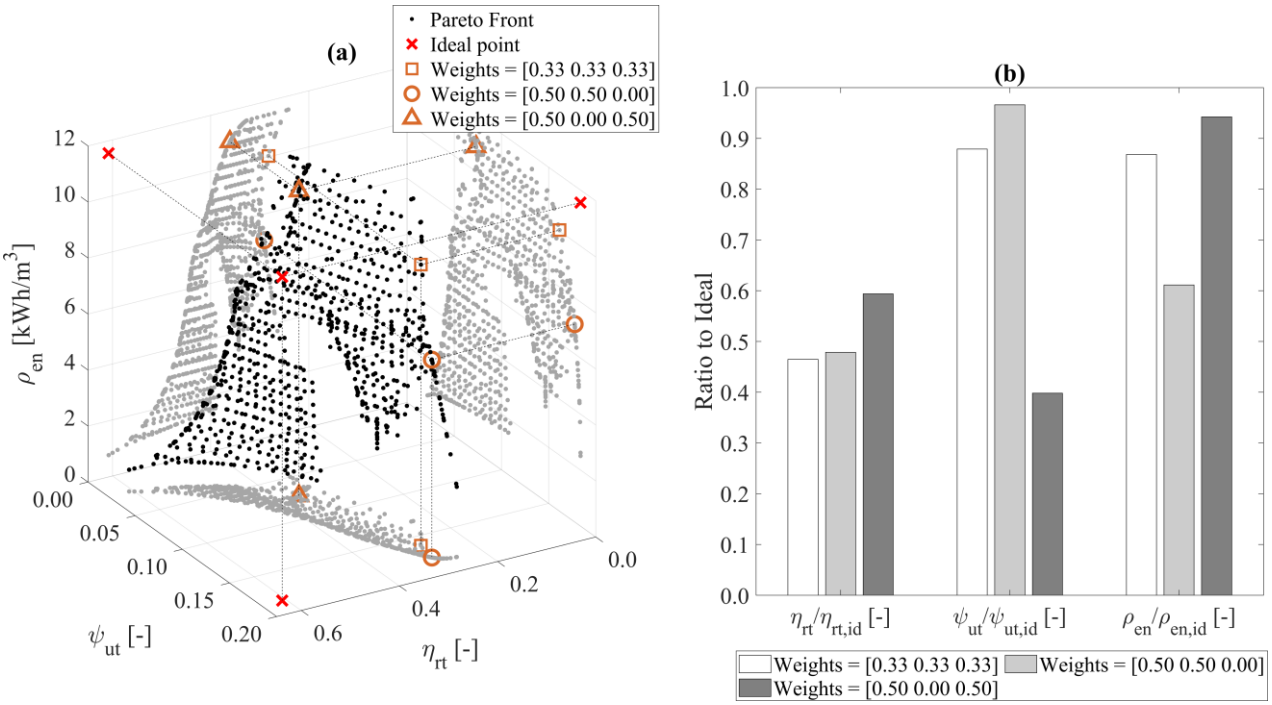

Figure 4. (a): Pareto front, ideal point and configurations corresponding to the three sets of weights $W_{1\text{-}3}$. (b): ratio between η_{rt}, ψ_{ut} and ρ_{en} and their respective ideal values: $\eta_{rt,id}$ = 0.608, $\psi_{ut,id}$ = 0.184 and $\rho_{en,id}$ = 11.552 kWh/m^3. Results are related to non-regenerated layout.

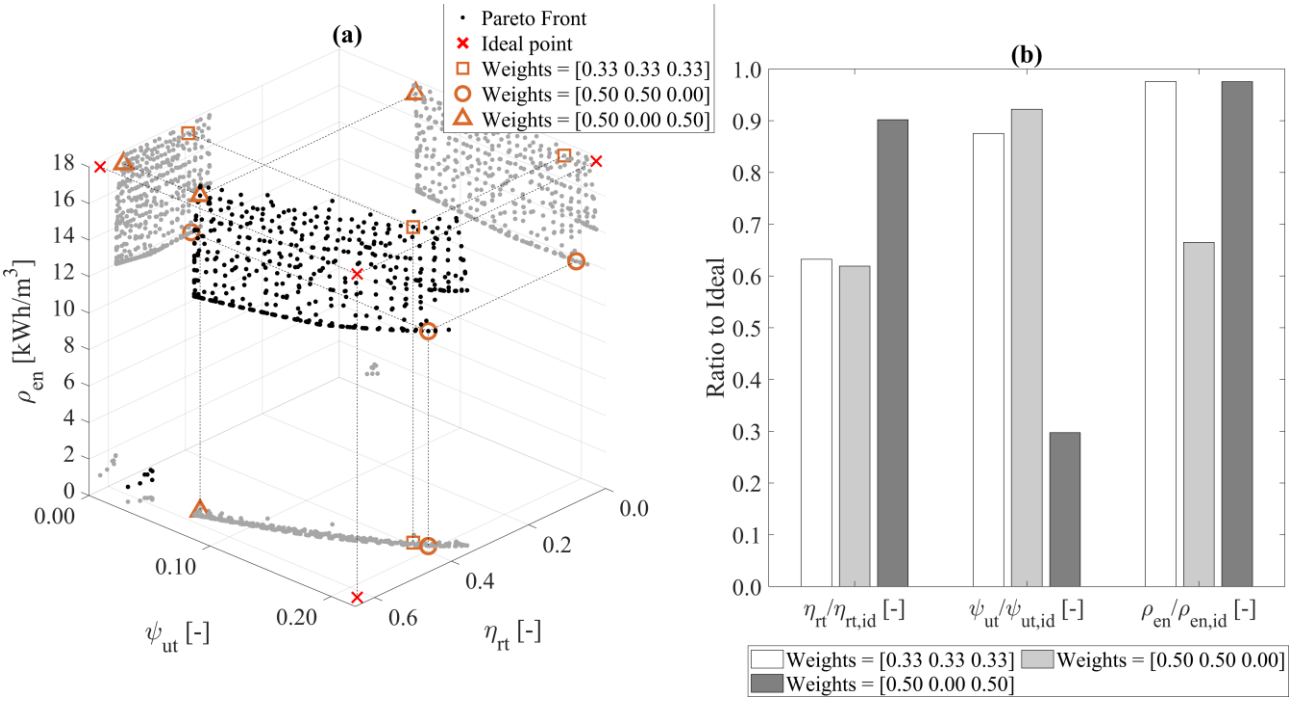

Figure 5. (a): Pareto front, ideal point and configurations corresponding to the three sets of weights $W_{1\text{-}3}$. (b): ratio between η_{rt}, ψ_{ut} and ρ_{en} and their respective ideal values: $\eta_{rt,id}$ = 0.621, $\psi_{ut,id}$ = 0.212 and $\rho_{en,id}$ = 17.722 kWh/m^3. Results are related to the regenerated layout.

As can be seen from Figures 4 (a) and 5 (a), the Pareto fronts are non-convex and discontinuous, and this justifies the use of a technique like that of Wierzbicki (Eq. 10) that can handle these situations. Non-convexity and discontinuity can arise due to strong non-linearities and constraints, which are both present in the investigated model. The regularity of the starting reference point grid is still visible in the arrangement of the Pareto front points. Furthermore, reference points which are located "far" from the actual front, or in correspondence of discontinuities, are all projected towards the nearest front region, thus forming zones in

which many points gather. For the same reason, Pareto front building process ends up with a significant number of duplicate points, which are filtered out and then not represented in Figures 4 (a) and 5 (a).
In both regenerated and non-regenerated cases, by specifying different weights, solutions well spread over the front are obtained. This can be either a positive or a negative feature, since it means that TI-PTESs are flexible systems, which can be tuned to promote the merit figure of interest. On the other hand, well-spread solutions mean that the trade-off between η_{rt}, ψ_{ut} and ρ_{en} is strong, then it is impossible to have a system that performs well in respect to all the performance parameters. In other words, high performance for η_{rt}, ψ_{ut} and ρ_{en} could be achieved, but at the cost of having poor performance according the other two.
One of the most significant differences between regenerated and non-regenerated cases can be observed by analyzing the Pareto front projection in the $\eta_{rt} - \psi_{ut}$ plane of Figures 4 (a) and 5 (a). In the non-regenerated case, the front projection is spread over a significant plane portion, suggesting that a non-negligible loss of performance is required, for having satisfactory values of ρ_{en}. This happens because the best combinations that can be achieved by only considering η_{rt} and ψ_{ut}, are those non-dominated among the front projection. These combinations correspond to the bi-dimensional Pareto front that would have been found if only η_{rt} and ψ_{ut} were considered. These combinations do not have the best ρ_{en}, since the objectives are competing. Thus, to achieve better ρ_{en}, the selected point must be vertically moved along the Pareto front surface. This tridimensional movement results in a bi-dimensional movement on the $\eta_{rt} - \psi_{ut}$ plane, that points away from the bi-dimensional pareto front towards worse η_{rt} and ψ_{ut} trade-offs.
In the regenerated case, front projection is almost collapsed over a line. This means that Pareto front surface is much steeper than in the non-regenerated case. Therefore, the trade-off between non-dominated combinations selected only according to η_{rt} and ψ_{ut}, and those selected considering also ρ_{en}, is weaker than in non-regenerated case.
In conclusion, being equal η_{rt} and ψ_{ut}, higher values are expected for ρ_{en} in the regenerated case, than in the non-regenerated one. This is valid in absolute terms, since regeneration naturally yields higher densities, as discussed before, but also in relative terms, when η_{rt}, ψ_{ut} and ρ_{en} are compared with their respective ideal counterparts. This conclusion is confirmed by the results reported in Figures 4 (b) and 5 (b) where it is clearly visible how, for similar relative values of ψ_{ut} and ρ_{en}, higher relative values of η_{rt} are achieved by the regenerated configuration. The most significant results, from this point of view, are those related with W_3. In this case, by passing from non-regenerated to regenerated layout, the ratio between η_{rt} and $\eta_{rt,id}$ changes from 0.6 to 0.9, while the ratio between ψ_{ut} and $\psi_{ut,id}$ changes only from 0.4 to 0.3 and that between ρ_{en} and $\rho_{en,id}$ remains roughly unchanged.
In Figure 6 (a − c) the combinations of η_{rt}, ψ_{ut} and ρ_{en} which correspond to W_1, W_2 and W_3 can be found. These performance indicators can be used to characterize the TI-PTES system and to compare it with other storage technologies.
In Figure 6 (a − c) regenerated and non-regenerated layouts are compared in absolute terms. For η_{rt} increments around 30% are found in case of W_1 and W_2, whereas increments around 35% are found for W_3. Much lower increments resulted for ψ_{ut}. For W_1, W_2 and W_3, increments around 15%, 10% and -13% are found. The fact that in some cases the regenerated layout performs worse than the non-regenerated one has to be seen more as an exception that as a rule. Furthermore, since the multi-criteria standpoint is assumed, triads of parameters should be compared together. Accordingly, regenerated W_3 configuration cannot be deemed as worse than its non-regenerated counterpart, since for a little decrease in ψ_{ut}, a relevant increase in both η_{rt} and ρ_{en} is achieved.
Finally, similarly to what resulted for single objective case, the major increments are registered for ρ_{en}: 70%, 67% and 59% are the increments related to W_1, W_2 and W_3, respectively. Therefore, ρ_{en} is confirmed as the most influenced parameter by regeneration.
In conclusion, even if the suitability of internal regenerator introduction must be investigated with a techno-economic analysis, it is clear that this modification is very promising. With respect to the basic layout, with a modest additional expenditure, much higher storage densities and much higher electric-to-electric efficiencies can be easily achieved.
Despite the performance increases due to the regeneration, the bottom line remains the same: it is possible to achieve η_{rt} higher than 50% and ρ_{en} around 17 kWh/m^3, but this can be done only if the heat source is unefficiently exploited. This could be a major hindrance to the further development of the TI-PTES technology, especially in those cases in which the thermal power is not readily available, as assumed here, and must be produced. This problem can be solved in many ways, ranging from layout modifications which allow for a better exploitation of heat source, to the use of working fluid mixtures, which could provide a better integration between the HTHP and the ORC. These are some aspects over which future researches should focus.

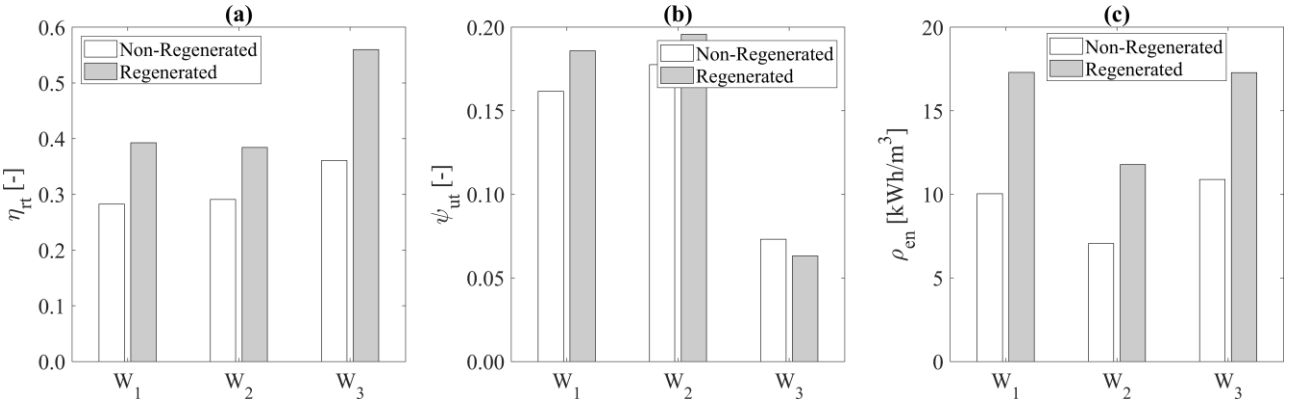

Figure 6. Comparison between the configurations corresponding to the three sets of weights $W_{1\text{-}3}$ for non-regenerated and regenerated layout. (a), (b) and (c) correspond to η_{rt}, ψ_{ut} and ρ_{en}, respectively.

The last thing is to compare TI-PTES with other storage technologies. For the sake of brevity, to perform this comparison, only the regenerated layout is considered.

As far as the energy density ρ_{en} is concerned, theoretical results suggest that values over 10 kWh/m^3 are always achieved, whereas values over 15 kWh/m^3 may be reached in some cases only. As specified in Section 2.2, ρ_{en} could be multiplied by a ½ factor if the total volume is considered. Whatever the case, TI-PTES shows densities higher than pumped-hydro and large-scale CAES, which have ρ_{en} between 0.5 and 2 kWh/m^3 and between 3 and 6 kWh/m^3[41]. Furthermore, resulting ρ_{en} is on the same level of that of liquid-air storage and slightly lower than of flow batteries (16 – 35 kWh/m^3) [41].

As far as η_{rt} is concerned, realistic values of this parameter suggested by theoretical results are between 0.4 and 0.57. These figures are slightly lower than that of CAES, which ranges from 0.45 to 0.7 and liquid-air storage, which are between 0.5 and 0.7 [41,42]. The comparison with PHES and flow batteries worse, as they usually achieve η_{rt} around 0.8 – 0.85.

As for ψ_{ut}, the only comparison that can be made is with CAES, since this is the only technology that integrates energy in forms other than the electric one, to the best of the authors' knowledge. The so-called diabatic CAES have total efficiency of around 0.54 [10]. This value is not calculated based on fuel chemical exergy, but since exergy and thermal power provided by fuel combustion are very similar, 0.54 is also indicative of the exergy efficiency of CAES. TI-PTES can achieve ψ_{ut} as high as 0.2, but realistic configurations more oriented towards having better η_{rt} might show ψ_{ut} as low as 0.07. The comparison with CAES, although based on a congruent indicator, is again somewhat incorrect. It is natural to have very low conversion efficiency while exploiting very low-grade thermal sources, like those used in the analysis ($T_{src,min} \leq 80$ °C). Furthermore, ψ_{ut} it is formulated considering also that the thermal energy of the source cannot be stored, so it gets wasted during storage idle periods, which is something that does not occur in CAES, as fuel is easily stored. Therefore, unlike η_{rt} and ρ_{en}, which can be used to compare TI-PTES with other storage technologies, ψ_{ut} is not fully suited to be used for comparison purposes. This parameter is to be used as an investigation tool, to understand the trade-offs that must be faced during TI-PTES theoretical design phase.

4. Conclusion

Based on the analysis that has been developed in previous sections, the following conclusions may be drawn. Two different configurations for a TI-PTES system, i.e. with and without internal regeneration, have been analyzed and compared. The theoretical thermodynamic design of the system has been performed by means of a nonlinear model, which is based on the resolution of a nonlinear constrained optimization problem. By changing the objective function, the system has been designed to promote different performance parameters, namely electric-to-electric efficiency η_{rt}, total exergy efficiency ψ_{ut} and energy density ρ_{en}. These parameters resulted to be competing with each other: high values of one of these, usually entails low values of the others. The definition of a flexible design tool and of a number of competing objectives, set the foundation for a multicriteria analysis which has been extensively performed. The main findings related to the first part of the analysis, which is based on single-objective optimization, can be summarized as follows:

- Maximum theoretical values for η_{rt}, ψ_{ut} and ρ_{en} can be achieved with the regenerated configuration and are equal to 0.65, 0.21 and 17.72 kWh/m^3. These values cannot be achieved concurrently;

- In the single-objective framework, regeneration introduction is very effective for ρ_{en}, as it leads to an increase of about 35%, whereas it is less effective for η_{rt}, which showed only a 6.5% increase, and ψ_{ut}, for which a 15% increase was found;
- By considering η_{rt}, ψ_{ut} and ρ_{en} as equally important, i.e. searching for "balanced" TI-PTES configurations, the most performing HTHP and ORC fluid pairs resulted to be Cyclopentane – Cyclopentane and R1336mzz(Z) – R1336mzz(Z) for regenerated and non-regenerated configuration, respectively.

The second part of the analysis is based on the multi-criteria analysis of the TI-PTES. Among non-dominated solutions, three configurations for each layout has been selected by specifying three different sets of objective weights, i.e. objective hierarchies. The main findings of the second part of the analysis can be summarized as follows:

- In the multi-objective framework, regeneration introduction resulted to be more effective, thus demonstrating its capability of relaxing trade-offs between objectives. By referring to three different sets of objective weights, the regenerated layout systematically achieves better objective configurations. If the same weight sets are compared, increments comprised between 30% and 35% can be achieved for η_{rt}, and between 60% and 70% for ρ_{en}. Maximum resulting ψ_{ut} increment is around 15%, but in one case a negative value, i.e. -13%, has been found. Such decrement is counterbalanced by high increments in both η_{rt} and ρ_{en}, thus leading to a globally better configuration;
- Given the resulting internal regeneration effectiveness, this layout modification has the potential to establish as the TI-PTES standard configuration. Despite this, this potentiality has to be verified with a dedicated techno-economic analysis, as the regeneration requires the introduction of two additional heat exchangers;
- Based on the multi-criteria analysis results, some TI-PTES theoretical performances can be derived. An interesting configuration could be the one related to the weight set W_3, which features η_{rt} roughly equal to 0.57 and ρ_{en} around to 17 kWh/m^3. Such levels of η_{rt} and ρ_{en} are a good achievement in terms of multi-objective optimization, since in this case the ratios η_{rt} / $\eta_{rt,id}$ and ρ_{en} / $\rho_{en,id}$ are both higher than 0.9. Given the required trade-off between objectives, this performance is paid in terms of ψ_{ut}, which was between 0.06 and 0.07, corresponding to a value of 0.3 in terms of ψ_{ut} / $\psi_{ut,id}$. If higher level of ψ_{ut} are required, i.e. $\psi_{ut} \approx 0.2$, ρ_{en} can be maintained high, $\rho_{en} \approx 17$ kWh/m^3, but η_{rt} must drop to 0.4;
- The performance suggested by theoretical analysis are promising if compared with other storage technologies. ρ_{en} was higher than that commonly featured by PHES and CAES, and roughly the same of that of flow batteries and liquid-air storage. For η_{rt} the comparison is less positive, since the theoretical analysis gave results that are slightly lower than those usually featured by technologies like CAES and liquid-air storage.

5. Acknowledgements

The authors deeply thank professor Alessio Artoni (Department of Civil and Industrial Engineering, at the University of Pisa) and Francesco Pistolesi (Researcher at Department of Information Engineering at the University of Pisa) for the lectures and the advices provided on multi-objective optimization and multi-criteria decision-making techniques. Without their contribution, the analysis would have been, if not impossible, at least much more difficult.

Appendix A

Upper and lower bounds set maximum and minimum, respectively, for each optimization variable. The related set of inequalities can be compactly written as in Eq. A.1:

$$\boldsymbol{LB} \leq \boldsymbol{x} \leq \boldsymbol{UB} \tag{A.1}$$

Where $\boldsymbol{LB}$, $\boldsymbol{UB}$ and $\boldsymbol{x}$ are the lower bound, upper bound and optimization variable vectors, respectively. $\boldsymbol{LB}$ and $\boldsymbol{UB}$ are reported in Eq. A.2a and A.3a, respectively, for the non-regenerated case and in Eq. A.2b and A.3b, respectively, for the regenerated case:

$$(\boldsymbol{LB})^{\boldsymbol{T}}|_{non-reg} = \{T_0 + PP_{hp,ev}; \max[T_0, T(p_{hp,min})]; T_0 + \Delta T_{hp,min}; 5; 5; T_0 + \Delta T_{hp,min}; \max[T_0 + \Delta T_{orc,sc}, T(p_{orc,min})]; 5; T_{src,max} + \Delta T_{src,min}; T_{src,max}\} \tag{A.2a}$$

$$(\boldsymbol{LB})^{\boldsymbol{T}}|_{reg} = \{(\boldsymbol{LB})^{\boldsymbol{T}}|_{non-reg}; 0\} \tag{A.2b}$$

$$(\boldsymbol{UB})^{\boldsymbol{T}}|_{non-reg} = \{T_{src,max} - \Delta T_{src,min}; T_{src,max} - \Delta T_{src,min} - PP_{hp,ev}; min(T_{hp,max}, T_{hp,crit}); 50; 50; min(T_{orc,max}, T_{orc,crit}); T_{src,max}; 30; T_{hp,max}; T_{hp,max}\} \tag{A.3a}$$

$$(\boldsymbol{UB})^{\boldsymbol{T}}|_{reg} = \{(\boldsymbol{UB})^{\boldsymbol{T}}|_{non-reg}; 50\} \tag{A.3b}$$

Where, apart from the symbols that have been already introduced, $\Delta T_{src,min} = T_{src,max} - T_{src,min}$ is the minimum heat source temperature difference that can be achieved in each configuration, $\Delta T_{hp,min} = T_{hp,cd} - T_{hp,ev}$ is the minimum HTHP temperature lift and $\Delta T_{orc,min} = T_{orc,ev} - T_{orc,cd}$ is the minimum ORC temperature drop.
For what concerns the optimization variables, their order in Eq. A.1 is the same as Section 2.3, so the vector $\boldsymbol{x}$ can be written as in Eq. A.4a for the non-regenerated case and in Eq. A.4b for the regenerated one:

$$(\boldsymbol{x})^T|_{non-reg} = \{T_{src,min}; T_{hp,ev}; T_{hp,cd}; \Delta T_{hp,sh}; \Delta T_{hp,sc}; T_{orc,ev}; T_{orc,cd}; \Delta T_{orc,sh}; T_{stg,max}; T_{stg,min}\} \tag{A.4a}$$

$$(\boldsymbol{x})^T|_{reg} = \{(\boldsymbol{x})^T|_{non-reg}; \Delta T_{orc,rg}\} \tag{A.4b}$$

For what concerns the linear constraints, they can be written as in Eq. A.5a–i

$$T_{hp,cd} - T_{hp,ev} \geq \Delta T_{hp,min} \tag{A.5a}$$
$$T_{hp,cd} - \Delta T_{hp,sc} - T_{stg,min} \geq PP_{hp,cd} \tag{A.5b}$$
$$T_{stg,max} - T_{stg,min} \geq \Delta T_{stg,min} \tag{A.5c}$$
$$T_{src,min} - T_{hp,ev} \geq PP_{hp,ev} \tag{A.5d}$$
$$T_{hp,ev} + \Delta T_{hp,sh} \leq T_{src,min} - PP_{hp,ev} \tag{A.5e}$$
$$T_{orc,ev} - T_{orc,cd} \geq \Delta T_{orc,min} \tag{A.5f}$$
$$T_{stg,max} - T_{orc,ev} - \Delta T_{orc,sh} \geq PP_{orc,ev} \tag{A.5g}$$
$$T_{orc,ev} + \Delta T_{orc,sh} \leq T_{orc,max} \tag{A.5h}$$

If the regenerated layout is to be considered, the set of linear constraints must be modified by dropping Eq. A.5e and by substituting it with Eq. A.5i:

$$T_{hp,cd} - T_{hp,ev} - \Delta T_{hp,sc} - \Delta T_{hp,sh} \geq PP_{hp,rg} \tag{A.5i}$$

Finally, for the non-linear constraints in the non-regenerated configuration, the following set of non-linear inequalities is considered (Eq. A.6a–m):

$$T_{cmp,out} - T_{hp,cd} \geq 0^2 \tag{A.6a}$$

[2] This constraint guarantees that the HTHP compressor performs dry compression.

$$T_{cmp,out} - T_{hp,max} \leq 0 \quad \text{(A.6b)}$$

Where $T_{cmp,out}$ is the temperature at the exit of the HTHP compressor.

$$T_{hp,cd} - PP_{hp,cd} - \left\{T_{stg,max} - \frac{\max[h_{cmp,out} - h_{sat,vap}(T_{hp,cd});\, 0]}{\Delta h_{hp,cd}} \cdot \left(T_{stg,max} - T_{stg,min}\right)\right\} \geq 0^{3} \quad \text{(A.6c)}$$

Where $h_{sat,vap}(T_{hp,cd})$ is the saturated vapor enthalpy evaluated at $T_{hp,cd}$, $\Delta h_{hp,cd}$ is the enthalpy difference across the refrigerant side of the HTHP condenser and $h_{cmp,out}$ is the enthalpy at the exit of the HTHP compressor.

$$COP - 1 \geq 0^{4} \quad \text{(A.6d)}$$

$$\chi_{exp,out} \geq 0.85 \quad \text{(A.6e)}$$

Where $\chi_{exp,out}$ is the vapor quality at the ORC expander exit.

$$T_{orc,ev} + PP_{orc,ev} - \left\{T_{stg,min} + \frac{h_{sat,liq}(T_{orc,ev}) - h_{pmp,out}}{\Delta h_{orc,ev}} \cdot \left(T_{stg,max} - T_{stg,min}\right)\right\} \geq 0^{5} \quad \text{(A.6f)}$$

Where $h_{sat,liq}(T_{orc,ev})$ is the saturated liquid enthalpy at $T_{orc,ev}$, $h_{pmp,out}$ is the enthalpy at the outlet of the ORC pump and $\Delta h_{orc,ev}$ is the enthalpy difference across the refrigerant side of the whole ORC evaporator.

$$T_{orc,cd} - PP_{orc,cd} - \left\{T_{air,out} - \frac{T_{air,out} - T_{air,in}}{\Delta h_{orc,cd}} \cdot \max\left[h_{exp,out} - h_{sat,vap}\left(T_{orc,cd}\right), 0\right]\right\} \geq 0^{6} \quad \text{(A.6g)}$$

Where $h_{exp,out}$ is the enthalpy at the exit of the ORC expander, $h_{sat,vap}(T_{orc,cd})$ is the saturated vapor enthalpy evaluated at $T_{orc,cd}$ and $\Delta h_{orc,cd}$ is the enthalpy difference across the refrigerant side of the ORC condenser.

$$T_{stg,max} - T_{stg,min} - \frac{\left(T_{hp,cd} - PP_{hp,cd} - T_{stg,min}\right) \cdot \Delta h_{hp,cd}}{h_{sat,vap}(T_{hp,cd}) - h(T_{hp,cd} - \Delta T_{hp,sc}; p_{hp,cd})} \leq 0 \quad \text{(A.6h)}$$

$$T_{cmp,out} - PP_{hp,cd} - T_{stg,max} \geq 0^{7} \quad \text{(A.6i)}$$

In case of internally regenerated configuration four additional constraints must be added, which are listed in Eq. A.6l–o:

$$T_{hp,cd} - \Delta T_{hp,sc} - \Delta T_{hp,rg} - PP_{hp,rg} - T_{hp,ev} \geq 0^{8} \quad \text{(A.6l)}$$

$$\Delta T_{orc,rg} \leq T_{exp,out} - T_{orc,cd}^{9} \quad \text{(A.6m)}$$

Where $T_{exp,out}$ is the temperature at the exit of the ORC expander.

$$T\left(p_{orc,ev}; h_{pmp,out}\right) - T_{exp,out} - \Delta T_{orc,rg} - PP_{orc,rg} \leq 0^{10} \quad \text{(A.6n)}$$

$$T\left(p_{orc,ev}; h_{pmp,out} + \Delta h_{orc,reg}\right) - T_{exp,out} - PP_{orc,rg} \leq 0^{11} \quad \text{(A.6o)}$$

where $\Delta h_{orc,reg}$ is the enthalpy difference between the cold side inlet and outlet in the ORC regenerator.

[3]This constraint enforces the observance of the pinch point at the beginning of condensation in the HTHP condenser.
[4]It can be demonstrated that this constraint, coupled with the others, guarantees the proper closing of the HTHP cycle.
[5]This constraint enforces the observance of the pinch point at the beginning of evaporation in the ORC evaporator.
[6]This constraint enforces the observance of the pinch point at the beginning of condensation in the ORC condenser.
[7]These two constraints guarantee the observance of energy balance and pinch point at the inlet (hot side) of the HTHP condenser.
[8]This constraint enforces the observance of the pinch point at the outlet (hot side) of the HTHP regenerator.
[9]Maximum achievable regeneration.
[10]This constraint enforces the observance of the pinch point at the outlet (hot side) of the ORC regenerator.
[11]This constraint enforces the observance of the pinch point at the inlet (hot side) of the ORC regenerator.

Appendix B

Table B1. η_{rt}, ψ_{ut} and ρ_{en} for all the investigated working fluid pairs in the non-regenerated layout. Best numerical results are underlined.

ORC Fluids:	Cyclo-pentane	Pentane	R1233zd(E)	R1224yd(Z)	R245fa	R1336mzz(Z)	R365mfc	R1234ze(E)
HTHP Fluids:	Round-trip efficiency – η_{rt} [-]							
Cyclo-pentane	<u>0.608</u>	0.586	0.585	0.577	0.578	0.575	0.579	0.585
Pentane	0.595	0.574	0.573	0.565	0.565	0.563	0.566	0.572
R1233zd(E)	0.591	0.570	0.569	0.561	0.562	0.560	0.563	0.569
R1224yd(Z)	0.585	0.564	0.563	0.555	0.556	0.554	0.557	0.563
R245fa	0.585	0.564	0.563	0.556	0.556	0.554	0.557	0.563
R1336mzz(Z)	0.589	0.568	0.567	0.559	0.560	0.558	0.561	0.567
R365mfc	0.592	0.571	0.570	0.562	0.563	0.561	0.564	0.570
R1234ze(E)	0.588	0.567	0.566	0.558	0.559	0.557	0.560	0.566
HTHP Fluids:	Heat source utilization efficiency – ψ_{ut} [-]							
Cyclo-pentane	<u>0.184</u>	0.165	0.165	0.158	0.157	0.157	0.159	0.161
Pentane	0.181	0.167	0.169	0.165	0.165	0.162	0.163	0.170
R1233zd(E)	0.175	0.163	0.164	0.162	0.163	0.159	0.159	0.167
R1224yd(Z)	0.170	0.158	0.160	0.156	0.157	0.154	0.155	0.161
R245fa	0.169	0.158	0.159	0.156	0.156	0.154	0.154	0.161
R1336mzz(Z)	0.177	0.165	0.167	0.164	0.165	0.161	0.161	0.170
R365mfc	0.179	0.165	0.167	0.163	0.164	0.160	0.161	0.169
R1234ze(E)	0.167	0.155	0.157	0.153	0.155	0.152	0.152	0.158
HTHP Fluids:	Energy density – ρ_{en} [kWh/m^3]							
Cyclo-pentane	11.552	12.218	12.585	12.946	13.069	12.599	12.345	<u>13.074</u>
Pentane	11.552	12.218	12.585	12.946	13.069	12.599	12.345	<u>13.074</u>
R1233zd(E)	11.552	12.218	12.585	12.946	13.069	12.599	12.345	<u>13.074</u>
R1224yd(Z)	11.552	12.218	12.585	12.946	13.069	12.599	12.345	<u>13.074</u>
R245fa	11.552	12.218	12.585	12.946	13.069	12.599	12.345	<u>13.074</u>
R1336mzz(Z)	11.552	12.218	12.585	12.946	13.069	12.599	12.345	<u>13.074</u>
R365mfc	11.552	12.218	12.585	12.946	13.069	12.599	12.345	<u>13.074</u>
R1234ze(E)	11.552	12.218	12.585	12.946	13.069	12.599	12.345	<u>13.074</u>

Table B2. η_{rt}, ψ_{ut} and ρ_{en} for all the investigated working fluid pairs in the regenerated layout. Best numerical results are underlined.

ORC Fluids:	Cyclo-pentane	Pentane	R1233zd(E)	R1224yd(Z)	R245fa	R1336mzz(Z)	R365mfc	R1234ze(E)
HTHP Fluids:	Round-trip efficiency – η_{rt} [-]							
Cyclo-pentane	0.630	0.645	0.621	0.623	0.622	0.641	<u>0.647</u>	0.610
Pentane	0.617	0.631	0.608	0.610	0.608	0.627	0.633	0.597
R1233zd(E)	0.613	0.627	0.604	0.606	0.604	0.623	0.629	0.593
R1224yd(Z)	0.606	0.621	0.598	0.599	0.598	0.616	0.623	0.586
R245fa	0.607	0.621	0.598	0.600	0.598	0.617	0.623	0.587
R1336mzz(Z)	0.611	0.625	0.602	0.604	0.602	0.621	0.627	0.591
R365mfc	0.614	0.628	0.605	0.607	0.605	0.624	0.630	0.594
R1234ze(E)	0.609	0.624	0.601	0.603	0.601	0.620	0.626	0.574
HTHP Fluids:	Heat source utilization efficiency – ψ_{ut} [-]							
Cyclo-pentane	0.208	0.205	0.192	0.191	0.190	0.200	0.203	0.186
Pentane	0.211	<u>0.211</u>	0.201	0.202	0.201	0.210	0.211	0.196
R1233zd(E)	0.204	0.208	0.204	0.206	0.206	0.211	0.209	0.201
R1224yd(Z)	0.196	0.201	0.197	0.204	0.205	0.205	0.202	0.196
R245fa	0.195	0.201	0.197	0.205	0.206	0.206	0.202	0.198
R1336mzz(Z)	0.207	0.211	0.205	0.207	0.206	0.212	0.212	0.201
R365mfc	0.209	0.210	0.200	0.201	0.201	0.209	0.209	0.196
R1234ze(E)	0.191	0.197	0.195	0.203	0.205	0.204	0.200	0.196
HTHP Fluids:	Energy density – ρ_{en} [kWh/m^3]							
Cyclo-pentane	13.636	16.492	16.175	17.535	17.690	<u>17.722</u>	17.282	16.351
Pentane	13.636	16.492	16.175	17.535	17.690	<u>17.722</u>	17.282	16.351
R1233zd(E)	13.636	16.492	16.175	17.535	17.690	<u>17.722</u>	17.282	16.351
R1224yd(Z)	13.636	16.492	16.175	17.535	17.690	<u>17.722</u>	17.282	16.351
R245fa	13.636	16.492	16.175	17.535	17.690	<u>17.722</u>	17.282	16.351
R1336mzz(Z)	13.636	16.492	16.175	17.535	17.690	<u>17.722</u>	17.282	16.351
R365mfc	13.636	16.492	16.175	17.535	17.690	<u>17.722</u>	17.282	16.351
R1234ze(E)	13.636	16.492	16.175	17.535	17.690	<u>17.722</u>	17.282	16.351

Table B3. Percentage increments of η_{rt}, ψ_{ut} and ρ_{en} for all the investigated working fluid pairs between the regenerated and non-regenerated layout.

ORC Fluids:	Cyclo-pentane	Pentane	R1233zd(E)	R1224yd(Z)	R245fa	R1336mzz(Z)	R365mfc	R1234ze(E)
HTHP Fluids:	Round-trip efficiency – $(\eta_{rt,reg} - \eta_{rt,non-reg})/\eta_{rt,non-reg} \cdot 100$ [-]							
Cyclo-pentane	3.681	10.073	6.161	7.925	7.563	11.319	11.865	4.236
Pentane	3.681	10.073	6.161	7.925	7.563	11.319	11.865	4.236
R1233zd(E)	3.681	10.073	6.161	7.925	7.563	11.319	11.865	4.236
R1224yd(Z)	3.681	10.073	6.161	7.925	7.563	11.319	11.865	4.236
R245fa	3.681	10.072	6.161	7.925	7.563	11.319	11.865	4.236
R1336mzz(Z)	3.681	10.073	6.161	7.925	7.563	11.319	11.865	4.236
R365mfc	3.681	10.073	6.161	7.925	7.563	11.319	11.865	4.236
R1234ze(E)	3.681	10.073	6.161	7.925	7.563	11.319	11.865	1.488
HTHP Fluids:	Heat source utilization efficiency – $(\psi_{ut,reg} - \psi_{ut,non-reg})/\psi_{ut,non-reg} \cdot 100$ [-]							
Cyclo-pentane	13.011	24.529	16.423	20.914	20.967	27.299	27.219	15.736
Pentane	16.602	26.852	19.034	22.374	21.912	29.754	29.566	15.412
R1233zd(E)	16.869	27.719	24.231	27.806	26.719	32.518	31.532	20.065
R1224yd(Z)	15.394	26.967	23.678	30.709	31.030	32.647	30.688	21.799
R245fa	15.495	27.052	23.885	31.644	31.940	33.621	30.941	22.812
R1336mzz(Z)	17.063	27.903	23.053	25.978	25.073	31.688	31.212	18.016
R365mfc	16.672	27.038	19.724	23.266	22.845	30.027	29.812	16.134
R1234ze(E)	14.601	26.769	24.363	32.759	32.071	34.603	31.770	23.794
HTHP Fluids:	Energy density – $(\rho_{en,reg} - \rho_{en,non-reg})/\rho_{en,non-reg} \cdot 100$ [-]							
Cyclo-pentane	18.044	34.987	28.529	35.441	35.360	40.654	39.992	25.061
Pentane	18.044	34.987	28.529	35.442	35.360	40.654	39.992	25.061
R1233zd(E)	18.044	34.987	28.529	35.441	35.360	40.654	39.992	25.061
R1224yd(Z)	18.044	34.987	28.529	35.441	35.360	40.654	39.992	25.061
R245fa	18.044	34.987	28.529	35.441	35.360	40.654	39.992	25.061
R1336mzz(Z)	18.044	34.987	28.529	35.441	35.360	40.654	39.992	25.061
R365mfc	18.044	34.987	28.529	35.441	35.360	40.654	39.992	25.061
R1234ze(E)	18.044	34.987	28.529	35.441	35.360	40.654	39.992	25.061

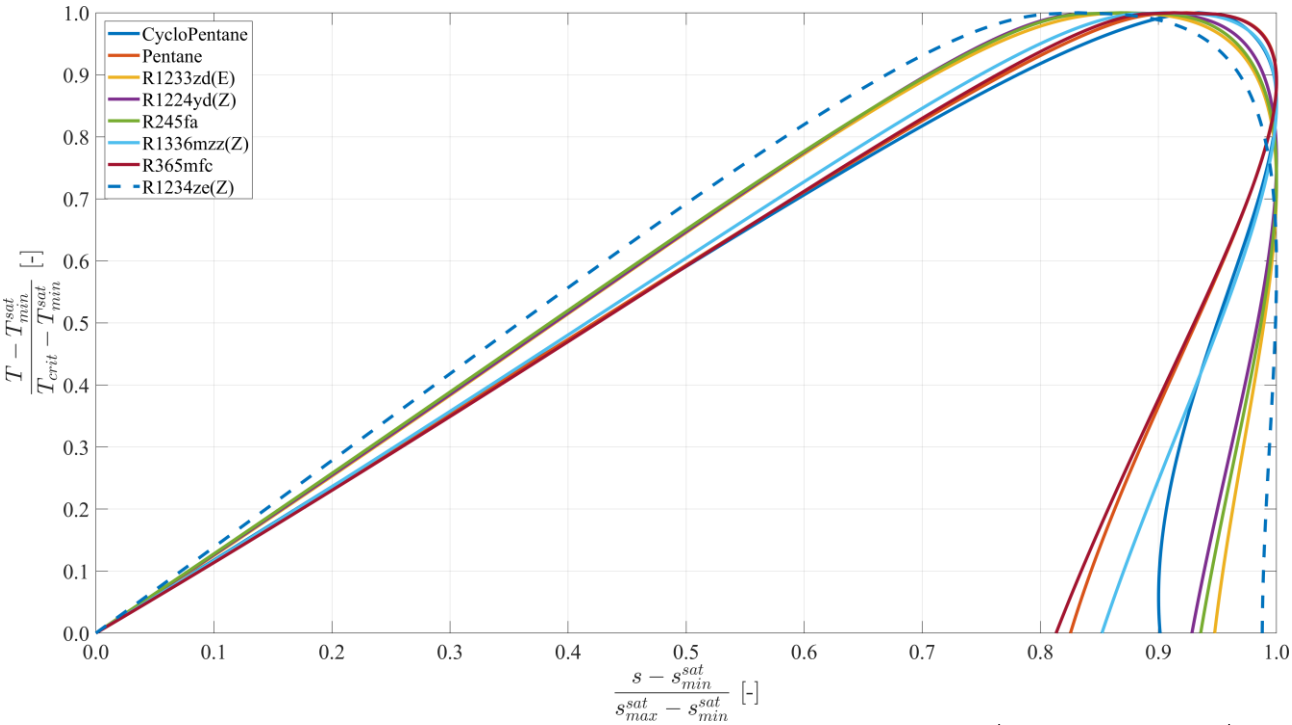

Figure B1. Normalized Ts diagram for the investigated TI-PTES working fluids. T_{min}^{sat}=413 K, while $s_{min}^{sat} = s(T_{min}^{sat}; \chi = 1)$ and s_{max}^{sat} is the maximum of the entropy achieved over the whole saturation line for $T_{sat} \geq T_{min}^{sat}$.

References

[1] Benato A, Stoppato A. Pumped Thermal Electricity Storage: A technology overview. Therm Sci Eng Prog 2018;6:301–15. doi:10.1016/j.tsep.2018.01.017.

[2] Frate GF, Antonelli M, Desideri U. Pumped Thermal Electricity Storage: An interesting technology for power-to-heat applications. 30th Int. Conf. Effic. Cost, Optim. Simul. Environ. Impact Energy Syst. ECOS 2017, International Measurement Confederation (IMEKO); 2017, p. 1–12.

[3] Frate GF, Antonelli M, Desideri U. A novel Pumped Thermal Electricity Storage (PTES) system with thermal integration. Appl Therm Eng 2017;121:1051–8. doi:10.1016/j.applthermaleng.2017.04.127.

[4] Desrues T, Ruer J, Marty P, Fourmigué JF. A thermal energy storage process for large scale electric applications. Appl Therm Eng 2010;30:425–32. doi:10.1016/j.applthermaleng.2009.10.002.

[5] Howes J. Concept and development of a pumped heat electricity storage device. Proc IEEE 2012;100:493–503. doi:10.1109/JPROC.2011.2174529.

[6] Benato A. Performance and cost evaluation of an innovative Pumped Thermal Electricity Storage power system. Energy 2017;138:419–36. doi:10.1016/j.energy.2017.07.066.

[7] Benato A, Stoppato A. Heat transfer fluid and material selection for an innovative Pumped Thermal Electricity Storage system. Energy 2018;147:155–68. doi:10.1016/j.energy.2018.01.045.

[8] Guo J, Cai L, Chen J, Zhou Y. Performance evaluation and parametric choice criteria of a Brayton pumped thermal electricity storage system. Energy 2016;113:693–701. doi:10.1016/j.energy.2016.07.080.

[9] White A, Parks G, Markides CN. Thermodynamic analysis of pumped thermal electricity storage. Appl Therm Eng 2013;53:291–8. doi:10.1016/j.applthermaleng.2012.03.030.

[10] Budt M, Wolf D, Span R, Yan J. A review on compressed air energy storage: Basic principles, past milestones and recent developments. Appl Energy 2016;170:250–68. doi:10.1016/j.apenergy.2016.02.108.

[11] Morandin M, Maréchal F, Mercangöz M, Buchter F. Conceptual design of a thermo-electrical energy storage system based on heat integration of thermodynamic cycles – Part A: Methodology and base case. Energy 2012;45:375–85. doi:10.1016/j.energy.2012.03.031.

[12] Morandin M, Maréchal F, Mercangöz M, Buchter F. Conceptual design of a thermo-electrical energy storage system based on heat integration of thermodynamic cycles – Part B: Alternative system configurations. Energy 2012;45:386–96. doi:https://doi.org/10.1016/j.energy.2012.03.033.

[13] Kim YM, Shin DG, Lee SY, Favrat D. Isothermal transcritical CO2 cycles with TES (thermal energy storage) for electricity storage. Energy 2013;49:484–501. doi:10.1016/j.energy.2012.09.057.

[14] Steinmann WD. The CHEST (Compressed Heat Energy STorage) concept for facility scale thermo mechanical energy storage. Energy 2014;69:543–52. doi:10.1016/j.energy.2014.03.049.

[15] Arpagaus C, Bless F, Schiffmann J, Bertsch SS. Multi-temperature heat pumps: A literature review. Int J Refrig 2016;69:437–65. doi:10.1016/j.ijrefrig.2016.05.014.

[16] Arpagaus C, Bless F, Uhlmann M, Schiffmann J, Bertsch SS. High temperature heat pumps: Market overview, state of the art, research status, refrigerants, and application potentials. Energy 2018;152:985–1010. doi:10.1016/j.energy.2018.03.166.

[17] Viking Heat Engines. Heatbooster n.d. http://www.vikingheatengines.com/heatbooster (accessed March 29, 2019).

[18] Frate GF, Ferrari L, Desideri U. Analysis of suitability ranges of high temperature heat pump working fluids. Appl Therm Eng 2019;150:628–40. doi:10.1016/J.APPLTHERMALENG.2019.01.034.

[19] Braimakis K, Karellas S. Energetic optimization of regenerative Organic Rankine Cycle (ORC) configurations. Energy Convers Manag 2018;159:353–70. doi:10.1016/j.enconman.2017.12.093.

[20] Steinmann WD. Thermo-mechanical concepts for bulk energy storage. Renew Sustain Energy Rev 2017;75:205–19. doi:10.1016/j.rser.2016.10.065.

[21] Peterson RB. A concept for storing utility-scale electrical energy in the form of latent heat. Energy 2011;36:6098–109. doi:10.1016/j.energy.2011.08.003.

[22] Reddy KS, Mudgal V, Mallick TK. Review of latent heat thermal energy storage for improved material stability and effective load management. J Energy Storage 2018;15:205–27. doi:10.1016/J.EST.2017.11.005.

[23] Zalba B, Marín JM, Cabeza LF, Mehling H. Review on thermal energy storage with phase change: Materials, heat transfer analysis and applications. Appl Therm Eng 2003;23:251–83. doi:10.1016/S1359-4311(02)00192-8.

[24] Ommen T, Jensen JK, Markussen WB, Reinholdt L, Elmegaard B. Technical and economic working

domains of industrial heat pumps: Part 1 – Single stage vapour compression heat pumps. Int J Refrig 2015;55:168–82. doi:10.1016/j.ijrefrig.2015.02.012.
[25] Quoilin S, Broek M Van Den, Declaye S, Dewallef P, Lemort V. Techno-economic survey of organic rankine cycle (ORC) systems. Renew Sustain Energy Rev 2013;22:168–86. doi:10.1016/j.rser.2013.01.028.
[26] Frate GF, Carro PP, Ferrari L, Desideri U. Techno-economic sizing of a battery energy storage coupled to a wind farm: An Italian case study. Energy Procedia, vol. 148, Elsevier; 2018, p. 447–54. doi:10.1016/j.egypro.2018.08.119.
[27] Frate GF, Peña Carro P, Ferrari L, Desideri U. On the suitability of a battery energy storage use in a wind farm. Proc. ecos 2018 - 31st Int. Conf. Effic. cost, Optim. Simul. Environ. impact energy Syst. June 17-22, 2018, Guimarães, Port., 2018.
[28] Zakeri B, Syri S. Electrical energy storage systems: A comparative life cycle cost analysis. Renew Sustain Energy Rev 2015;42:569–96. doi:10.1016/j.rser.2014.10.011.
[29] Dumont O, Quoilin S, Lemort V. Design, Modeling and Experimentation of a Reversible HP-ORC Prototype, 2014. doi:10.1115/gt2014-26854.
[30] Dumont O, Quoilin S, Lemort V. Experimental investigation of a reversible heat pump/organic Rankine cycle unit designed to be coupled with a passive house to get a Net Zero Energy Building. Int J Refrig 2015;54:190–203. doi:10.1016/J.IJREFRIG.2015.03.008.
[31] Dumont O, Carmo C, Fontaine V, Randaxhe F, Quoilin S, Lemort V, et al. Performance of a reversible heat pump/organic Rankine cycle unit coupled with a passive house to get a positive energy building. J Build Perform Simul 2018;11:19–35. doi:10.1080/19401493.2016.1265010.
[32] MathWorks. Constrained Nonlinear Optimization Algorithms n.d. https://it.mathworks.com/help/optim/ug/constrained-nonlinear-optimization-algorithms.html#f26684 (accessed April 11, 2019).
[33] Bell IH, Wronski J, Quoilin S, Lemort V. Pure andPseudo-pure Fluid Thermophysical Property Evaluation and the Open-SourceThermophysical Property Library CoolProp. Ind Eng Chem Res 2014;53:2498–508. doi:dx.doi.org/10.1021/ie4033999.
[34] Lemmon EW, Bell IH, Huber ML, McLinden MO. NIST Standard Reference Database 23: Reference Fluid Thermodynamic and Transport Properties-REFPROP, Version 10.0, National Institute of Standards and Technology 2018. doi:https://dx.doi.org/10.18434/T4JS3C.
[35] Wierzbicki AP. The Use of Reference Objectives in Multiobjective Optimization, 2012. doi:10.1007/978-3-642-48782-8_32.
[36] Deb K, Sundar J, Udaya Bhaskara RN, Chaudhuri S. Reference Point Based Multi-Objective Optimization Using Evolutionary Algorithms. Int J Comput Intell Res 2010;2. doi:10.5019/j.ijcir.2006.67.
[37] Kontomaris K. HFO-1336mzz-Z: High Temperature Chemical Stability and Use as A Working Fluid in Organic Rankine Cycles. Int Refrig Air Cond Conf 2014:10.
[38] Molés F, Navarro-Esbrí J, Peris B, Mota-Babiloni A, Barragán-Cervera Á, Kontomaris K. Low GWP alternatives to HFC-245fa in Organic Rankine Cycles for low temperature heat recovery: HCFO-1233zd-E and HFO-1336mzz-Z. Appl Therm Eng 2014;71:204–12. doi:10.1016/j.applthermaleng.2014.06.055.
[39] Hwang CL, Lai YJ, Liu TY. A new approach for multiple objective decision making. Comput Oper Res 1993;20:889–99. doi:10.1016/0305-0548(93)90109-V.
[40] Kumar A, Sah B, Singh AR, Deng Y, He X, Kumar P, et al. A review of multi criteria decision making (MCDM) towards sustainable renewable energy development. Renew Sustain Energy Rev 2017;69:596–609. doi:10.1016/j.rser.2016.11.191.
[41] Luo X, Wang J, Dooner M, Clarke J. Overview of current development in electrical energy storage technologies and the application potential in power system operation. Appl Energy 2015;137:511–36. doi:10.1016/j.apenergy.2014.09.081.
[42] Aneke M, Wang M. Energy storage technologies and real life applications – A state of the art review. Appl Energy 2016;179:350–77. doi:10.1016/j.apenergy.2016.06.097.